Spring 5-7-2018

A speleothem record of climate variability in Southwestern North America during Marine Isotope Stage 3

Justin G. Peinado

Justin G. Peinado

Candidate

Earth and Planetary Science, University of New Mexico

Department

This thesis is approved, and it is acceptable in quality and form for publication:

Approved by the Thesis Committee:

Yemane Asmerom, Chair

Victor Polyak

Joseph Galewsky

A SPELEOTHEM RECORD OF CLIMATE VARIABILITY IN SOUTHWESTERN NORTH AMERICA DURING MARINE ISOTOPE STAGE 3

BY

JUSTIN PEINADO

B.S. General Geology, Northern Arizona University, 2014

THESIS

Submitted in Partial Fulfillment of the
Requirements for the Degree of

Master of Science in Earth and Planetary Sciences
July, 2018

The University of New Mexico
Albuquerque, New Mexico

DEDICATION

This thesis is dedicated to my grandfather, Arnold Peinado. I want to thank him for always supporting me and instilling in me an interest in Geology and Chemistry.

A SPELEOTHEM RECORD OF CLIMATE VARIABILITY IN SOUTHWESTERN NORTH AMERICA DURING MARINE ISOTOPE STAGE 3

By

Justin G. Peinado

B.S., School of Earth Sciences and Environmental Sustainability, Northern Arizona University, 2014

Master of Science in Earth and Planetary Sciences, University of New Mexico, 2018

ABSTRACT

During Marine Isotope Stage 3 (MIS-3) of the last glacial period, there were rapid transitions between warm and cold climates referred to as Dansgaard-Oeschgerr (DO) events. In Southwestern North America (SWNA), two speleothem paleoclimate records document changes in moisture source delivery in response to DO-events during MIS-3, but do not address potential changes in effective moisture for the region. In this study, we introduce a new high-resolution speleothem paleoclimate record from Carlsbad Cavern in the Guadalupe Mountains. The speleothem, sample BC-5, grew continuously from 46-31 kya during the latter half of MIS-3, based on U-Th dating. We also tied stable isotope ($\delta^{18}O$ and $\delta^{13}C$) and trace element (Sr/Ca, Mg/Ca, and Ba/Ca) analysis to the U-series chronology to produce multiple high-resolution time-series. Our data further strengthens the shifting westerly storm-track hypothesis and suggest that DO-events led to changes in effective moisture. The stable isotope time-series displays DO-events and are clearly tied to other speleothem records from SWNA and the NGRIP ice core record. When compared to a Holocene speleothem record (BC-11) and a speleothem Asian Monsoon

record, it becomes apparent that $\delta^{13}C$ is a record of local changes in effective moisture and vegetation. $\delta^{13}C$ also suggests an atmospheric pCO_2 control on vegetation and speleothem calcite during the last glacial as has been suggested in other studies. Trace element analysis of BC-5 further supports the stable isotope interpretations. Sr/Ca, Mg/Ca, and Ba/Ca all strongly covary, indicating that they are controlled by similar processes, and are likely connected to changes in effective moisture and local karst processes.

TABLE OF CONTENTS

LIST OF FIGURES

LIST OF TABLES

CHAPTER I INTRODUCTION

Southwestern North America (SWNA) is currently a semi-arid to arid, drought sensitive region that depends on two sources of moisture: Pacific-derived winter moisture and the North American Monsoon (NAM; Seager & Vecchi 2010; Macdonald 2010). Two important speleothem records from the region, Asmerom et al. (2010) and Wagner et al. (2010), document moisture source variability in response to dramatic climate change events throughout the last glacial period. These records are primarily moisture source indicators and provide a hemispherical link, but do not clearly tie changes in moisture source variability to changes in effective moisture (precipitation minus evaporation) during these events.

This study is aimed at understanding effective moisture variability in SWNA during well-documented hemispheric climate change events observed in the Greenland Ice Cores during Marine Isotope Stage-3 (MIS-3) of the last glacial. To achieve this, a new high-resolution speleothem paleoclimate record is constructed using stalagmite BC-5 from Carlsbad Cavern in the Guadalupe Mountains of SWNA. Sample BC-5 was collected from a ventilated, or “unstable”, cave setting and uranium-series ages show that it grew continuously from 46-31 ka, providing a 15-ky paleoclimate record from the latter half of MIS-3. In contrast to the previous speleothem studies from SWNA, the setting that BC-5 grew in has a more direct connection with surface climate and may have made the sample more susceptible to changes in surface conditions and will provide a better record of effective moisture variability than previous studies.

1.1 – Northern Hemisphere Climate Variability during the Last Glacial

The last glacial period lasted from ~75-15 kya, and at the core of the last glacial was Marine Isotope Stage 3 (MIS-3). MIS 3 was a relatively warm period that lasted from ~60-25 kya and is characterized by pronounced climate variability as recorded in ice core, marine and continental proxies globally (Allen & Anderson 1993; Wang et al., 2001; Oster et al., 2015; Bohm et al., 2015). This climate variability is recognized as reoccurring episodes of cold reversals followed by episodes of rapid warming in the north Atlantic, referred to as Dansgaard-Oeschger (DO) events. In addition to DO-events were dramatic glacial discharge episodes known as Heinrich events. Synchronicity of these events in numerous paleoclimate proxies has generated research aimed at understanding their impact on climate systems throughout the Northern Hemisphere and globe (Rasmussen et al., 2014).

DO-events are decadal-scale shifts in the isotopic ($\delta^{18}O$) and elemental composition (Ca^{2+}) of ice layers that are observed in the GISP, GISP 2, and NGRIP ice cores from the Greenland ice sheet (Rasmussen et al., 2014; Dansgaard, 1993). These DO- and Heinrich events are interspersed by millennial-scale periods of relatively warm and cold climates that occurred in the north Atlantic, which are referred to as Greenland interstadials (GI) and stadials (GS), respectively. A mechanism for the dramatic and rapid shifts seen during DO-events remains uncertain, but it is widely accepted that they represent changes in average annual air temperature of between 5-10°C and shifting of the polar jet around the north Atlantic (Dansgaard et al., 1993). Timing of events has been shown to strongly correlate with paleoclimate proxies throughout the northern

Hemisphere (Zhou et al., 2014; Burns et al., 2003; Gallego-Torres et al., 2014), suggesting that the events lead to or represent dramatic changes in climate.

Heinrich events are identified as ice rafted debris (IRD) layers in northern Atlantic Ocean sediment cores that were deposited by glacial armadas from the Laurentide ice sheet. These events resulted in or coincided with dramatic cooling in the northern hemisphere, sea level rise, weakening or shutdown of North Atlantic Deep Water (NADW) formation, and atmospheric reconfiguration (Bond et al., 1992; Heinrich 1988; Brunier & Brook, 2001; Hemming et al., 2004; Guihou et al. 2010). IRD events are thought to take place immediately preceding or during GS's, but issues with dating ice rafted debris (IRD) layers and the time-transgressive nature of Heinrich events makes defining the onset and ending of glacial discharge episodes difficult (Hemming et al., 2004; Stanford et al., 2011; Austin and Hibbert 2012). Regardless of their timing, the resulting climate shifts following the events is seen in numerous paleoclimate proxies. Heinrich events coincide with stadials, but not all stadials are associated with IRD layers.

Continental paleoclimate records throughout North America show climate responses to Heinrich and DO-events as evidenced by pluvial lake episodes (Reheis et al., 2014) along the western U.S., the stalagmite records of Asmerom et al. (2010) and Wagner et al. (2010) in the southwestern U.S., and changes in vegetation in the mid-west (Dorale et al., 1998) and southeastern U.S. (Grimm et al., 1993). In China, a notable speleothem record documents changes in monsoonal strength in response to DO events and Heinrich stadials (Wang et al., 2001). A speleothem record from the Alps also suggests a tightly coupled climate between Europe and Greenland (Mosely et al., 2014). In general, climate variability seems to be well-documented during the last glacial throughout the Northern Hemisphere. However, there is still difficulty in determining the exact timing and nature of regional climate responses. Especially in continental interiors where high-resolution, centennial- or decadal-scaled paleoclimate records are sparse (Voelker et al., 2001).

1.2 – Modern Climate of Southwestern North America

Carlsbad Cavern is located in arid to semi-arid SWNA, at latitudes 32.18°N and longitude -104.44°E. At present, the region relies heavily on moisture from the North America Monsoon summer moisture and less frequent Pacific-derived winter moisture (Seager et al., 2007). These sources of moisture are currently modulated by decadal-scale variability of sea surface temperatures and atmospheric circulation (Shepperd et al., 2002; Stewart et al., 2005). Paleoclimate studies have documented the presence and variability of these moisture sources throughout the Holocene and into the latter half of the last glacial. Of these studies, multiple speleothem-based climate records have come from the Guadalupe Mountains of SWNA (Polyak and Asmerom, 2001; Polyak et al., 2001; Polyak et al., 2004; Rasmussen et al., 2006; Asmerom et al., 2007; Asmerom et al., 2013).

Carlsbad Cavern is situated in the Guadalupe Mountains, which are located in southeast New Mexico and West Texas near the boundary of the Chihuahuan desert. In the past 30 years, the NAM has accounted for over 60% of precipitation in the range and surrounding area, with rainfall beginning in late July and ending in early September (Adams and Comrie, 1997; Castro et al., 2001). Like other monsoonal systems, insolation-driven heating of the continental interior during the late summer shifts the prevailing wind direction, resulting in moisture laden air being drawn into the continental interior from the Gulf of Mexico and Gulf of California. The presence of a subtropical high-pressure ridge to the east of SWNA also aids in pumping moisture laden air into the region. The size and location of this high-pressure ridge is influenced by the Inter-Tropical Convergence Zone (ITCZ). The ITCZ is a band of low-pressure driven by equatorial heating that moves north and south from the equator in response to hemispheric cooling or heating (Haug et al., 2001; Chiang & Bitz 2005).

In contrast, Pacific-derived winter moisture is controlled by cooling of the Northern Hemisphere and movement of the polar jet stream. The polar jet stream is a narrow band of fast-moving westerly winds, and its location is controlled by the temperature gradient between the North Pole and the equator. Southward movement of the polar jet stream as the Northern Hemisphere begins to cool during the winter months leads to a shift in the westerly storm track. This results in moisture being drawn into the continent from the Pacific Ocean. Precipitation from Pacific-derived winter moisture and the NAM have unique isotopic compositions, due to the timing and mechanisms of their delivery. Precipitation from the NAM typically has $\delta^{18}O$ values of between 2-3‰, and precipitation from Pacific-derived winter storms have a $\delta^{18}O$ of around -11‰ (Hoy & Gross, 1982; Yapp, 1985). This largely results from the distillation effect, as Pacific moisture travels a far greater distance than the NAM, resulting in rainout of the heavy isotope and enrichment of the lighter isotope.

Amount of moisture delivered from the Pacific is modulated by decadal-scale climate oscillations, referred to as the El Nino Southern Oscillation (ENSO) and the

Pacific Decadal Oscillation (PDO) (Mantua et al., 1997). Periods of positive ENSO and PDO correlate to increased winter precipitation for SWNA due to a more southerly and zonal polar jet. This is attributed to relatively warm sea surface temperatures (SST) in the Pacific Ocean around the equator.

Southward displacement of the winter storm track results in drier conditions in the northwestern United States, and wetter conditions in SWNA. The relationship between these two systems and their effect on winter precipitation has been observed and measured over the past century (Latif and Barnett, 1996). However, the link between ENSO and PDO to the NAM is not as pronounced, and it appears that the NAM is largely independent of these oscillations. Regardless, the presence and effects of ENSO and PDO have been documented in the late to mid Holocene in a variety of proxies (Anderson et al., 1992; Gray et al., 2003; Rasmussen et al., 2006; Asmerom et al., 2013), but their presence into the early Holocene and last glacial remains largely unknown.

1.2 – Climate of SWNA during the Last Glacial

The Estancia Basin lacustrine record is perhaps the best record of SWNA climate for the last glacial but lacks a high-resolution chronology during MIS-3 (Allen & Anderson, 2000). This record documents millennial-scale changes in pluvial lake levels into the early Holocene. Lake high-stands, or relatively wet periods, are attributed to an increase in Pacific-derived winter moisture during GS's, and the opposite is seen during GI's. A speleothem $\delta^{18}O$ record (stalagmite FS-2) from Fort Stanton cave in Southern New Mexico also seemingly shows an increase in winter moisture during GS's and a decrease during GI's but is primarily a record of moisture source and not effective moisture (Asmerom et al., 2010) during MIS-3. Another speleothem $\delta^{18}O$ record from Cave of the Bells (stalagmite COB) in Southern Arizona shows similar moisture source variability during MIS-3 (Wagner et al., 2010).

The shift to a Pacific-derived winter moisture source during GS's seen in each of these records is attributed to a strengthened and southward shifted polar jet delivering more winter moisture to SWNA. This explanation has been tested and verified in a variety of climate models focused on the Last Glacial Maximum (LGM) (Arpe et al., 2011). Additionally, the presence of the Laurentide ice sheet over northern North America during the last glacial has also been shown to influence the polar jet due to the presence of a high-pressure system over the ice sheet (Oster et al., 2015). This is further supported by lacustrine paleoclimate records from along the west coast (Reheis et al., 2014). Overall, continental paleoclimate records suggest an increase in winter moisture delivery during GS's due to a more southerly and zonal winter storm track. However, the changes in moisture source have not been clearly tied to changes in effective moisture in SWNA during MIS-3.

1.3 – The Cave Setting

The Guadalupe Mountains hosts the Capitan Reef, which is a world-renowned example of a Permian fossil reef system. It is also home to world famous caves, Carlsbad Cavern and Lechuguilla Cave, which are located within thick sequences of limestone and dolostone associated with the backreef, reef, and forereef. At present, >300 caves have been documented in the mountains, many of which formed by a sulfuric acid-related process (Hill 2000). This process of speleogenesis, now known as a type of hypogene speleogenesis, produced caves that are described as having large, vertical entrances with large, well-ventilated passages that are heavily decorated (Hill 1987). Speleothems from caves in the mountains provide an excellent opportunity for paleoclimate research given the climate, geographic location and geomorphology of the area.

Of the various speleothem types, stalagmites have been shown to be the most viable for paleoclimate reconstructions in the Guadalupe Mountains (Polyak and Asmerom, 2001; Rasmussen et al., 2006; Asmerom et al., 2013). In general, as calcite precipitates to form a stalagmite it is often precipitated as recognizable bands or lamina, like growth rings seen in tree ring records. Lamina, as in tree rings, represent varying periods of growth and the chemical (elemental and isotopic) composition of the lamina reflects environmental conditions during the period of calcite precipitation. The process of speleothem growth begins as rain/snow precipitation that penetrates into and through soil. Precipitation reacts with soil CO_2 and becomes slightly acidic due to the formation of H_2CO_3. This water can then infiltrate the limestone bedrock where it will dissolve calcium carbonate. This will release calcium (Ca^{2+}) and bicarbonate (HCO_3^-) ions into solution as it travels through various paths and reservoirs until it reaches the cave ceiling. At this point, the CO_2-charged solution will likely have a significantly higher $p$$CO_2$ than the cave atmosphere, which will lead to degassing of CO_2 and the precipitation of calcium carbonate in the form of calcite or aragonite. The complete reaction is as follows:

Rainwater reacting with soil CO_2,

$$H_2O + CO_2 \rightarrow H_2CO_3$$

Dissolution of bedrock,

$$CaCO_3 + H_2CO_3 \rightarrow Ca^{2+} + 2HCO_3^-$$

Degassing and calcite/aragonite precipitation,

$$Ca^{2+} + 2HCO_3^- \rightarrow CaCO_3 + H_2O + CO_2$$

The calcite/aragonite of speleothems can be absolutely dated using uranium-series dating techniques. This allows for construction of a high-resolution chronology, which can then be tied to stable isotope and elemental measurements. Stalagmites are the preferred speleothem type because they tend to grow continuously along a vertical axis and the growth rate is relatively high in comparison to other speleothems. $\delta^{18}O$ and $\delta^{13}C$ are commonly measured stable isotopes, and barium (Ba), magnesium (Mg), and strontium (Sr) are commonly measured trace elements. Stable isotope and elemental concentrations in speleothem calcite are controlled by a multitude of processes at the surface and subsurface. Due to the numerous processes that control stable isotope and elemental concentrations, an understanding of the mechanics at play in the karst setting where the speleothem grew is important.

The sulfuric acid hypogene caves of the Guadalupe Mountains, including Carlsbad Cavern, are large and spacious and usually have a single large entrance. Because of this, the environment in these caves is somewhat evaporative, since dry, cold air from the surface is seasonally sinking into the cave and displacing the warm, humid cave air. Thus, stalagmites, like stalagmite BC-5, grow in an evaporative cave environment, Conditions during the last glacial were probably more cold and wet, which could have promoted less evaporation in comparison to the modern cave environment. However, it also important to note that MIS-3 was a period of complex climate history, with many well-documented climate change events that may have had significant effects on karst processes and the resulting speleothem calcite. Analysis of stalagmites, particularly from Batcave Passage, from Carlsbad Cavern should then reveal a unique climate history.

CHAPTER II METHODS

This study used uranium-series dating methods to construct a high-resolution chronology for stalagmite BC-5 from Carlsbad Cavern. Stable isotope measurements of $\delta^{18}O$ and $\delta^{13}C$, in addition to trace element measurements of Mg, Ba, and Sr, were measured and tied to the uranium-series chronology to produce high-resolution time-series. These time-series will serve as paleoclimate proxies that record a variety of climate signals and karst processes. Furthermore, comparison of the BC-5 record to the well-established Greenland ice core proxies (NGRIP, GRIP, and GISP2), Fort Stanton speleothem $\delta^{18}O$ record (FS-2), and other paleoclimate proxies will allow for interpretation of potential regional climate responses to hemispheric climate change events.

2.1 – Sample BC-5

Sample BC-5 was collected from Bat Cave passage, not far from the entrance of Carlsbad Cavern (Fig. 01). Measurements in Bat Cave passage of atmospheric pressure, relative humidity (RH), drip rate, pCO_2 and trace element concentrations in drip waters were performed by Rasmussen (2006). In this cave passage, air stagnates during the summer months resulting in relatively high pCO_2, temperatures, and RH. In contrast, the cave more actively ventilates during the winter months (late fall to early spring) as colder air from the surface sinks into the passage and displaces cave air (McClean 1971). The passage is evaporative due to the active ventilation during most of the year, and RH typically averages 85-90% annually. This allows cave drip waters to experience some degree of evaporation throughout the year. However, this is also dependent on the timing and rate of drip waters entering the cave. Drip waters in the summer are exposed to less evaporation as compared to drip waters in the winter when ventilation is active and RH is more similar to the surface RH. Previous studies on stalagmites from Carlsbad Cavern and other caves in the Guadalupe Mountains showed a significant connection between the cave and surface climate throughout the Holocene (Rasmussen et al., 2006; Asmerom et al., 2007; Asmerom et al., 2013). These studies highlighted the use of Guadalupe Mountain stalagmite annual band, $\delta^{18}O$, and $\delta^{13}C$ records as effective moisture indicators.

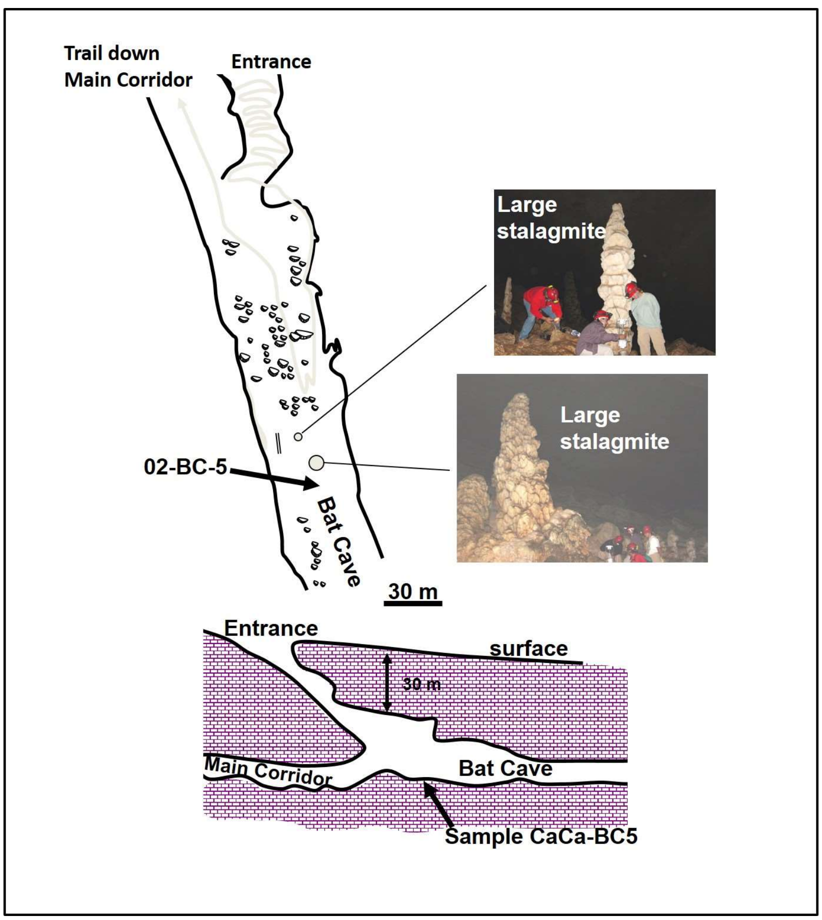

Figure 01: Diagram of Bat Cave passage in Carlsbad Cavern showing the location sample BC-5 was collected from.

The stalagmite studied in Asmerom et al. (2013), stalagmite BC-11, grew ~30m from stalagmite BC-5 and recorded climate variability going back ~1500 years from present.

Stalagmite BC-5 is 390 mm in length and 80 mm in diameter (Fig. 2). The stalagmite has a slight yellowish-orange color compared to the more grey/white late Holocene samples from this part of the cave (Fig. 3). The color likely represents greater amounts of soil organic compounds, comparable to stalagmites from caves at higher more forested elevations in the Guadalupe Mountains. Layering is visible throughout the stalagmite and a grayscale time-series was constructed to show the growth characteristics

Figure 02: Cut section of BC-5, showing the interior of the stalagmite.

of the stalagmite. There is also a notable hiatus at around 306 mm (fig. 4), and this appears to be the only hiatus of any significance.

Figure 03: BC-11 (Late Holocene - upper) and BC-5 (Last Glacial - bottom)

Figure 04: Thin section of BC-5 around a hiatus (black band and darker calcite), near the bottom of the stalagmite. This section is 36.8 mm long. The rest of the speleothem has no other major hiatus's such as this one, but may contain smaller, less-noticeable ones. Annual banding can also be seen in this section (alternating layers of dark and white bands).

2.2 - Radiometric dating of BC-5

Description of the uranium-series system

The densely crystalline calcite/aragonite composition of speleothem lamina provides an excellent opportunity for construction of high-resolution uranium-series chronologies. In the uranium-238 decay chain, ^{238}U decays to ^{230}Th through multiple daughters that also undergo radioactive decay. The complete uranium-series decay chain is as follows:

$$^{238}U > {}^{234}Th > {}^{234}Pa > {}^{234}U > {}^{230}Th.$$

The relatively short half-lives of ^{234}Th and ^{234}Pa do not contribute any significant time and can be ignored. Therefore, the isotopes that need to be considered when determining age are ^{238}U, ^{234}U and ^{230}Th (Dorale et al., 2007). The radioisotopes of uranium are soluble under oxidizing conditions in soil and bedrock, so they are readily mobilized in water at earth's surface conditions. However, thorium is not soluble under typical surface conditions and is largely immobile. Therefore, water moving through soil and carbonate bedrock is capable of mobilizing uranium, but not thorium. The resulting cave drip waters and speleothem carbonates are then relatively enriched in uranium as compared to thorium. What little detrital thorium is incorporated into the stalagmites carries with it minute amounts of ^{230}Th that is not part of the decay from initial ^{238}U in the stalagmite carbonate and is easily corrected for in most circumstances. This makes the uranium-series system ideal for dating speleothem carbonates. The half-life of the daughter in this system, ^{230}Th, is 75,584 ± 110 years and makes this method capable of dating calcite/aragonite up to ~650,000years before present (Edwards et al., 2003; Cheng et al., 2013).

In radioactive decay, secular equilibrium is reached when the decay rate or activity of each daughter is equal to the activity of the parents. That is, the quantity of the daughter isotopes relative to the parent isotopes remains constant and no longer changes over time since the production rate is equal to the decay rate. Typical radiogenic dating techniques measure the accumulation of the radiogenic or stable daughter to determine age. However, in the uranium-series system the degree of secular equilibrium that has been reached is used to determine age. This is because the daughter, ^{230}Th, is radioactive and also decays. Relative to time, secular equilibrium in the uranium-series system can be described using the following equation:

$$\frac{dN_{230}}{dt} = -\lambda_{230} N_{230} + \lambda_{234} N_{234} + \lambda_{238} N_{238}$$

In this equation, N_x is the number of atoms present for the respective isotope x, λ_x is the decay constant, which is the fraction of the number of atoms that decay in one second, and *t* is time in seconds. To determine age using the uranium-series method in a speleothem carbonate, the following expanded equation can be used:

$$\left(\frac{^{230}Th}{^{238}U}\right)_A = (1 - e^{-\lambda_{230} t}) + \frac{\lambda_{230}}{(\lambda_{230} - \lambda_{234})} * (\gamma_0 - 1) * (e^{-\lambda_{234} t} - e^{-\lambda_{230} t})$$

This equation describes the evolution of the system where $(^{230}Th/^{238}U)_A$ is an activity (A) ratio and γ_0 is initial $(^{234}U/^{238}U)_A$, which is almost always a measurement of disequilibrium in the speleothem system. Since the carbonates in speleothem lamina can be considered a closed system after deposition, we can correct for initial thorium by assuming the amount incorporated from soil and/or bedrock. This initial value is also referred to as the detrital component, and the detrital ^{230}Th to be removed to measure corrected ages is determined by measuring the concentration of ^{232}Th.

Preparation and Measurements

BC-5 was cut parallel to the growth axis and ~100 mg powders along lamina were drilled at 20 mm increments down the growth axis, from 0 to 360 mm. In addition, five powders were drilled at 108.5 mm to attempt an isochron age to determine initial $^{230}Th/^{232}Th$ values. Powders were dissolved in nitric acid (HNO_3) and mixed with a ^{229}Th-^{233}U-^{236}U spike. ^{229}Th-^{233}U-^{236}U are synthetic isotopes, not found in nature. Uranium and thorium were separated in 2 ml anion exchange columns using conventional anion-exchange chromatography. Eichrom 1x8, 200-400 mesh chloride form anion resin was used in the columns, which contains 0.5 ml of resin. Once separated and dried, samples were re-dissolved in 3% nitric acid. Separately, samples of uranium and thorium were measured as ratios using a Thermo Neptune multi-collector inductively coupled plasma mass spectrometer (MC-ICP-MS) at the University of New Mexico Radiogenic Isotope Laboratory.

The Neptune MC-ICP-MS has switchable Faraday cup resistors with four 10^{12} Ω resistors for low intensity signals, five 10^{11} Ω resistors for normal intensity signals, one 10^{10} Ω resistor for high intensity signals, and a secondary electron multiplier (SEM) for counting very low signals. The SEM or Faraday cup - 10^{12} Ω resistor set up in the center position was used to measure the least abundant isotopes, which are ^{234}U and ^{230}Th (Asmerom et al. 2006). For example, signals of 5mV or less (1mV = 62,500 cps) were measured using the SEM detector. A gain or efficiency value between the SEM and Faraday cups must be measured with the sample measurements. The Neptune is also coupled to an Aridus II desolvating nebulizer, which increases the signal by 4 times. The uranium standard NBL-112 and a ^{230}Th in-house standard were measured to control the gain between the SEM and Faraday cups. Procedural blanks are ~10 pg and ~30 pg for Th and U, respectively.

2.3 - Stable Isotope Measurements

For stable isotope measurements, 1 mg powders were drilled at a continuous 1 mm resolution. In total, 360 samples were drilled and measured for $\delta^{18}O$ and $\delta^{13}C$. Measurements were made by Mathew S. Lachniet at the Las Vegas Isotope Science Laboratory in the Department of Geosciences at the University of Nevada using their Thermo Electron Delta V Plus mass spectrometer. $\delta^{18}O$ and $\delta^{13}C$ are reported in per mil notation (‰) due to a large difference between the abundances of oxygen-18 and oxygen-16. The equation for $\delta^{18}O$ is as follows:

$$\delta^{18}O = \left(\frac{\left(\frac{^{18}O}{^{16}O} \right)_{sample}}{\left(\frac{^{18}O}{^{16}O} \right)_{s\tan dard}} - 1 \right) * 1000‰$$

The equation for $\delta^{13}C$ is similar, except that it is comparing carbon-13 to carbon-12. Delta values are reported versus the international Vienna Pee Dee Belemnite (VPDB) standard.

Processes that could shift carbon and/or oxygen isotopic compositions are deposition of calcite out of isotopic equilibrium (i.e., kinetic fractionation due to an evaporative cave environment), evaporation of water at or near the land surface, physical and chemical interactions between ground water and bedrock prior to calcite deposition, and a change in the source of moisture (Hendy, 1971). A common method of evaluating the degree to which speleothem calcite was deposited out of equilibrium is by calculating a correlation coefficient between $\delta^{18}O$ and $\delta^{13}C$, referred to as the Hendy test. Non-equilibrium conditions are thought to lead to a positive correlation, and close to 0 or negative correlation for equilibrium conditions. However, this test has fallen under scrutiny in recent years, and may not be a reliable indicator of non-equilibrium fractionation (Dorale & Liu, 2009; Wong & Breeker, 2015). This may be the case specially in situations where $\delta^{18}O$ and $\delta^{13}C$ are being controlled by similar environmental factors, leading to positive correlation in equilibrium conditions. A Hendy test was not performed for stalagmite BC-5.

Under equilibrium conditions, $\delta^{13}C$ is largely controlled by the degree to which bedrock dissolution and prior calcite precipitation (PCP) occurs (Deines et al., 1974). Both result in more positive, or heavier $\delta^{13}C$ values. Measurements of bedrock $\delta^{13}C$ in the Guadalupe Mountains showed values between 3-8‰ (Hill, 1996). $\delta^{13}C$ may also reflect changes in vegetation and soil CO_2 as the relative proportion of isotopically light C3 and isotopically heavy C4 plants changes above the cave (Dorale et al., 1998). Recent $\delta^{13}C$ work has focused on the effect of atmospheric pCO_2 concentrations on speleothem calcite, and highlight changes of -2‰ or more from the LGM-Holocene transition (Wong & Breeker 2015). The mechanisms behind the observed shifts in multiple speleothem records remain ambiguous and is attributed to a variety of factors in the epikarst and karst (Wong & Breeker 2015). In contrast, $\delta^{18}O$ values of speleothems are generally not significantly influenced by bedrock, since HCO_3 in cave dripwaters is mostly derived from meteoritic precipitation (Harmon 1979).

2.4 - Elemental Measurements

For trace element measurements, a 2mm drill bit was used to drill powders in a continuous transect from the top to the bottom of BC-5, from 1 to 305 mm, producing 150 powders (Fig. 05). Powders were dissolved in a few drops of 7N nitric acid and diluted 5000-10000 times with a 3% nitric acid solution spiked with an internal standard, indium (In), so that the final solution had a 10 ppb In concentration. Analyses were performed on the Thermo X Series ICP-MS at the University of New Mexico Radiogenic Laboratory. ICP-MS standards containing Ca, Mg, Sr, Ba, and U were measured before and after every twenty samples were analyzed. The standards were made from a 10 ppm stock solution of Inorganic Ventures IV-ICPMS 71, a multielement ICP standard. Calibration curves were made from analyzing 1000, 500, 200, 100, 50, 20, and 5 ppb dilutions of this standard.

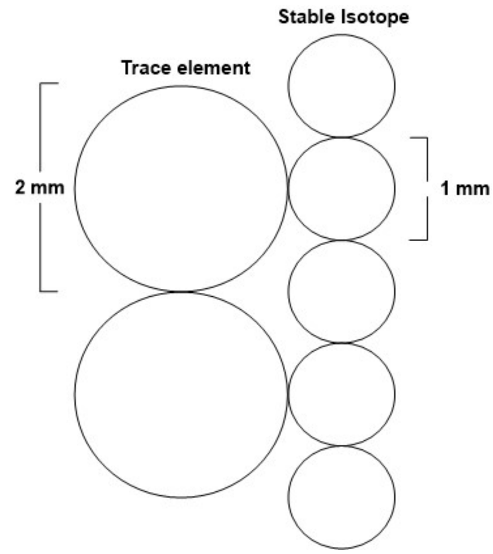

Figure 5: Diagram of the elemental drill hole sizes (2mm) in comparison to the stable isotope measurements that were at 1mm resolution.

Trace element concentrations in speleothems are dependent on the chemical composition of cave drip waters and physical conditions (temperature, RH, and pCO_2) of the cave environment during calcite precipitation. Like stable isotopes, the trace element composition of cave drip waters is controlled by the interaction of infiltrating waters with bedrock. In arid, moisture-limited regions, this interaction is heavily influenced by the residence time of infiltrating waters in bedrock (Fairchild et al., 2000; Tremaine & Froelich 2013).

Dry periods typically correspond to slower infiltration rates, increased water-bedrock interaction, and subsequently high concentrations of Mg, Sr, and Ba in cave drip waters. These relatively high concentrations are attributed to bedrock dissolution and degassing of waters stored in the karst system, which leads to PCP. PCP increases the ratio of trace elements relative to calcium, as most trace elements have a partition coefficient of less than one and are not selectively removed from solution (Fairchild & Treble 2009). Typically, positive correlation of trace elements and stable isotopes is thought to be a strong indication of PCP or increased water-bedrock interactions, which reflects relatively dry climates (Cruz et al., 2007; Sinclair et al, 2012). Recent work has also shown that elemental concentrations in active cave drip waters show a clear correlation to surface temperatures (Casteel & Banner 2015). Since trace element concentrations and stable isotope ratios can be influenced by similar mechanisms, comparison of data sets allows for further interpretation of the controls on each system (Johnson et al., 2006; Oster et al, 2012).

2.5 – Grayscale Measurements

Grayscale is simple to measure and can provide a record of exceptionally high-resolution growth variability. A highly resolved reflected-light scan of stalagmite BC-5 was processed using Digital Micrograph, a computer program for making measurements in electron microscopy. A grayscale histogram of a reflected light image was made for a transect along the center of the growth axis that was 200 pixels wide (~14 mm wide). A wide swath normalizes anomalies in grey and essentially filters out small artifacts. The histogram was tied to the uranium-series age control to produce a grayscale time-series that represents changes in stalagmite growth, which should directly produce important climate periodicities through spectral analysis.

2.6 - Statistical Analyses

An age model was constructed using COPRA (Breitenbach et al. 2012) in MATLAB to produce the stable isotope, elemental, and grayscale time-series. Spectral analysis of the time series was performed using REDFIT, which was developed by Schulz & Mudelsee (2001). REDFIT is a Fortran 90 program that fits a first-order autoregressive process to unevenly spaced time-series. Isotope and elemental time-series measured in stalagmites are not evenly spaced due to the nature of sample growth. REDFIT can interpolate between measurements in a time series without altering estimated spectrum by enhancing high or low frequency components. This allows for identification of periodicities in each time-series.

CHAPTER III RESULTS

3.1 – BC-5 Chronology

The final chronology for stalagmite BC-5 includes 21 ages (Table 01). A powder drilled at the top, at 11 mm, gave an age of 31,433.36 with a 2-sigma (2σ) error of ± 246. Near the bottom of the stalagmite, at 330 mm, an age of 52,587 ± 204 was obtained. Between 313 mm and 301 mm, at approximately 306 mm, there is a hiatus where no growth occurred between 52-46 kya. The pre-hiatus ages, ranging from 360-306, were not stratigraphically consistent, but define a roughly thousand-year brief period of growth

Table 01: BC-5 Uranium-series analysis

mm from top	^{238}U (ng/g)	^{232}Th (pg/g)	$^{230}Th/^{232}Th$ activity ratio	$^{230}Th/^{238}U$ activity ratio	$\delta^{234}U$ (‰) measured	$\delta^{234}U$ (‰) initial	Uncorrected age yrs BP	Corrected age yrs BP
11	452±0.2	752±32	999±43	0.5437±0.0012	1095±2.1	1197±2.3	31895±85	31433±246
29.5	460±0.3	617±33	1268±69	0.5558±0.0012	1098±2.1	1204±2.3	32656±87	32220±235
49	538±0.4	175±30	5291±917	0.5631±0.0012	1070±2.1	1177±2.3	33663±91	33368±181
70	269±0.2	249±45	1911±342	0.5769±0.0014	1061±2.1	1170±2.3	34798±105	34163±353
90	457±0.3	295±46	2778±438	0.5853±0.0013	1060±2.1	1172±2.3	35381±98	34995±225
102	413±0.3	2271±35	338±5	0.6095±0.0013	1072±2.1	1190±2.3	36819±101	36189±330
110	374±0.3	697±61	1010±88	0.6159±0.0017	1060±2.1	1179±2.3	37518±131	36962±310
116	1155±0.7	898±61	2450±166	0.6234±0.0015	1065±2.1	1185±2.3	37946±116	37578±150
130	444±0.3	200±42	4252±885	0.6283±0.0013	1051±2.1	1172±2.3	38602±107	38233±226
149	470±0.3	758±50	1230±81	0.6493±0.0021	1082±2.1	1209±2.4	39410±154	38967±271
168	488±0.6	1114±5	878±40	0.6553±0.0015	1052±2.1	1179±2.3	40537±122	40071±263
190	470±0.3	539±39	1771±129	0.6644±0.0014	1038±2.0	1167±2.3	41536±116	41114±243
213.5	502±0.4	1228±41	848±28	0.6784±0.0019	1026±2.0	1158±2.3	42875±152	42659±186
226	627±0.4	960±41	1342±57	0.6727±0.0014	994±2.0	1123±2.3	43287±122	43125±146
240.5	557±0.6	179±36	6494±1309	0.6841±0.0016	1016±2.0	1149±2.3	43578±129	43287±203
260	653±0.3	429±41	3221±305	0.6925±0.0014	1028±2.0	1163±2.3	43890±121	43598±191
283	528±0.3	461±39	2454±206	0.7001±0.0015	1015±2.0	1152±2.3	44803±125	44435±224
293	644±0.5	167±32	4797±598	0.7013±0.0015	1002±2.0	1139±2.3	45257±133	45008±207
301	691±1.2	230±37	6423±1032	0.6999±0.0018	987±2.0	1122±2.3	45573±154	45481±161
313	627±0.4	427±51	3545±421	0.7892±0.0017	986±2.0	1145±2.4	52763±155	52457±220
330	653±0.4	171±38	9209±2026	0.7901±0.0017	987±2.0	1145±2.4	52834±154	52587±204

at 52,800 years ago. The laminae below the hiatus are wavy, powdery, and ill-defined. This is interpreted as alteration of the original calcite for this early period of growth.

From 306 to 0 mm, continuous growth is assumed, averaging 0.022 mm/year based on the COPRA generated time-series. There is a small portion of the stalagmite, from 43.5-42.5 kya, where the growth rate increased dramatically to 0.06-0.08 mm/year. Growth rates this high are supported by annual band measurements sporadically throughout the stalagmite. The final chronology used and uranium-series ages are shown in fig.06.

Five powders drilled at 108.5 mm to produce an isochron to determine a curve for

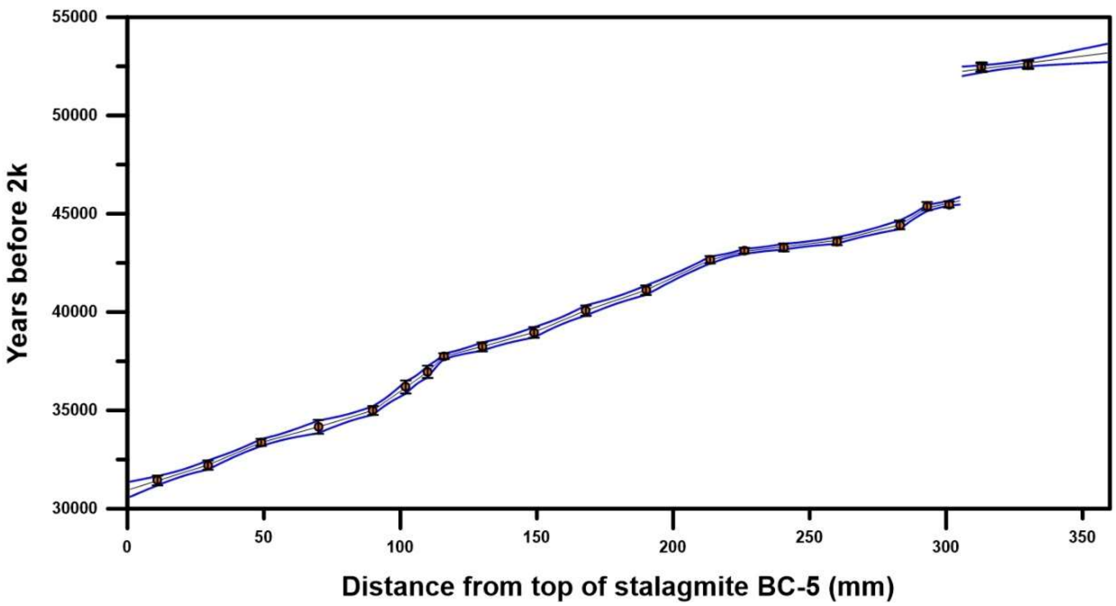

Figure 06: Uranium-series ages (orange circles) with error bars. The blue lines are the error envelopes produced from COPRA, and the black line connecting Uranium-series ages is the chronology used.

the input of initial $^{230}Th/^{232}Th$ values for age corrections was not successful because of the lack of spread in values. The data for these five samples are in table 02. Poor spread in values produces a large error size. The initial chronology based thorium values measured using a non-linear initial $^{230}Th/^{232}Th$ versus ^{232}Th correction curve for Holocene samples by Rasmussen (2006) produced a chronology that was offset just beyond the range of age errors when compared to the GRIP and FS-2 records. While the isochron did not work out, the results suggested a high initial $^{230}Th/^{232}Th$ value for this sample. Therefore, the non-linear correction curve used by Rasmussen (2006) was modified to allow for three times higher initial $^{230}Th/^{232}Th$ values on the low ^{232}Th concentration end of the curve, which corrected the ages and shifted the BC-5 record to match FS-2 and GRIP. The correction curve used was $y = 0.1192 (x^{-0.985})$, where x = ^{232}Th concentration in ppt, and y = initial $^{230}Th/^{232}Th$ value. The higher initial $^{230}Th/^{232}Th$ values used in the BC-5 chronology is probably related to higher contributions of detrital ^{230}Th from the bedrock during the late glacial period. Overall, the initial thorium values derived from the correction curve produced a more reasonable match.

Table 02: Isochron data for stalagmite BC-5

Mm from top	^{238}U (ng/g)	^{232}Th (pg/g)	$^{230}Th/^{232}Th$ activity ratio	$^{230}Th/^{238}U$ activity ratio	$\delta^{234}U$ (‰) measured	$\delta^{234}U$ (‰) initial	Uncorrected age yrs BP	Corrected age yrs BP
108.5(a)	410±0.3	608±54	1164±103	0.5647±0.0014	907±2.1	1007±2.3	37206±117	36981±163
108.5(b)	376±0.3	657±34	990±51	0.5672±0.0015	909±1.9	1010±2.2	37333±123	37081±177
108.5(c)	416±0.3	738±64	977±85	0.5675±0.0013	907±1.9	1008±2.1	37427±109	37190±162
108.5(d)	381±0.3	546±37	1208±82	0.5672±0.0017	912±1.9	1013±2.2	37270±139	37036±182
108.5(e)	381±0.3	615±44	1073±76	0.5666±0.0013	902±1.9	1003±2.1	37460±111	37215±166

3.2 – Stable isotope and Elemental time-series

$\delta^{18}O$ and $\delta^{13}C$ time-series are listed in table 03 and shown in figure 07. Oxygen isotope values range from -3.65 to -7.25‰, with a total range of 3.6‰. Carbon isotope values range from -0.25 to -5.14‰, with a total range of 4.85‰. These ranges are based on all the isotopic measurements. However, measurements near the hiatus and near the top/bottom of the stalagmite are markedly heavier. This is interpreted as due to alteration of the calcite during periods when growth ceased, and the calcite was exposed to the cave air coming in and out and producing a hydration rind. These values were removed, as they are not representative of true climate mechanisms. In graphing the results, values near the top of the stalagmite and near the hiatus were removed.

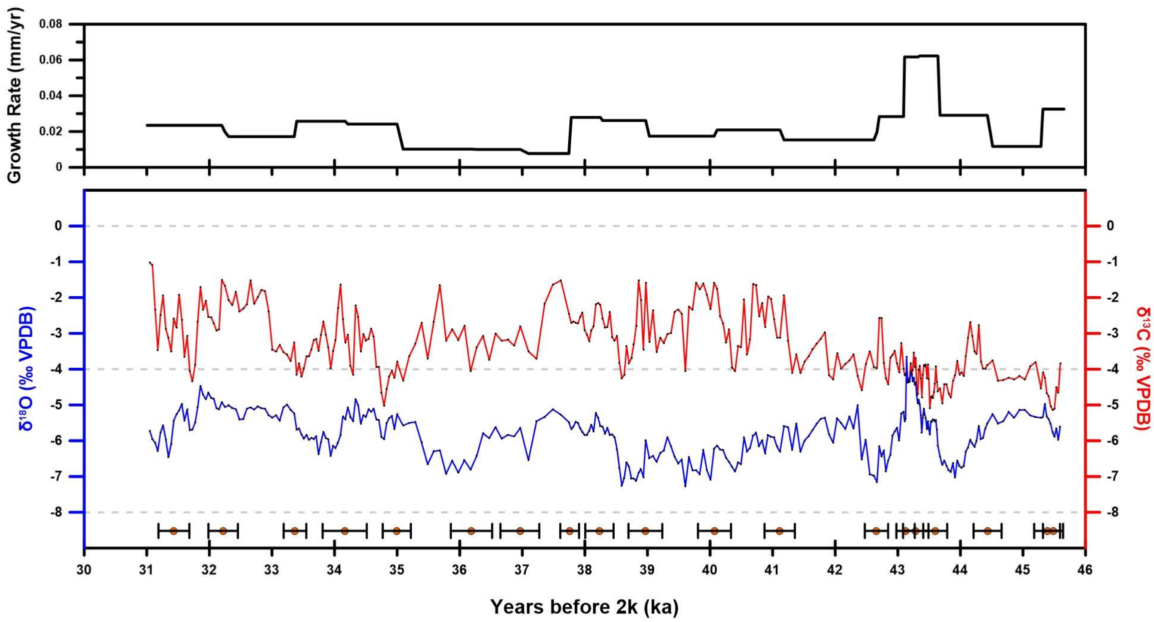

<u>Figure 07</u>: BC-5 oxygen and carbon time-series (bottom) with growth rate taken from the COPRA chronology (top). Orange circles are Uranium-series ages with errors bars.

After the hiatus, from 46 to 31 ka, overall correlation between oxygen and carbon is low with a correlation coefficient (*r*) of 0.017. Pre-hiatus correlation between oxygen and carbon is high ($r = 0.9$, $p < 0.001$), and values are relatively heavy as compared to the rest of the record (fig. 08). Additional correlation coefficients were also calculated at various sub-intervals and shown with the growth rate in fig.09 with some periods having high correlations.

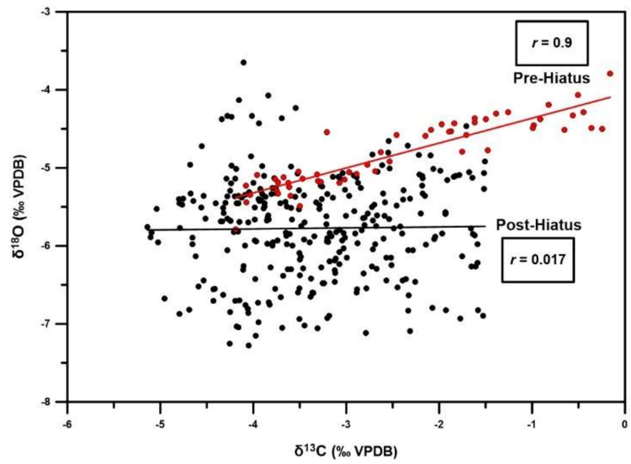

Figure 08: Correlation of $\delta^{18}O$ and $\delta^{13}C$ in BC-5. Red points are pre-hiatus measurements (r = 0.09, p < 0.001), and black points are post-hiatus measurements.

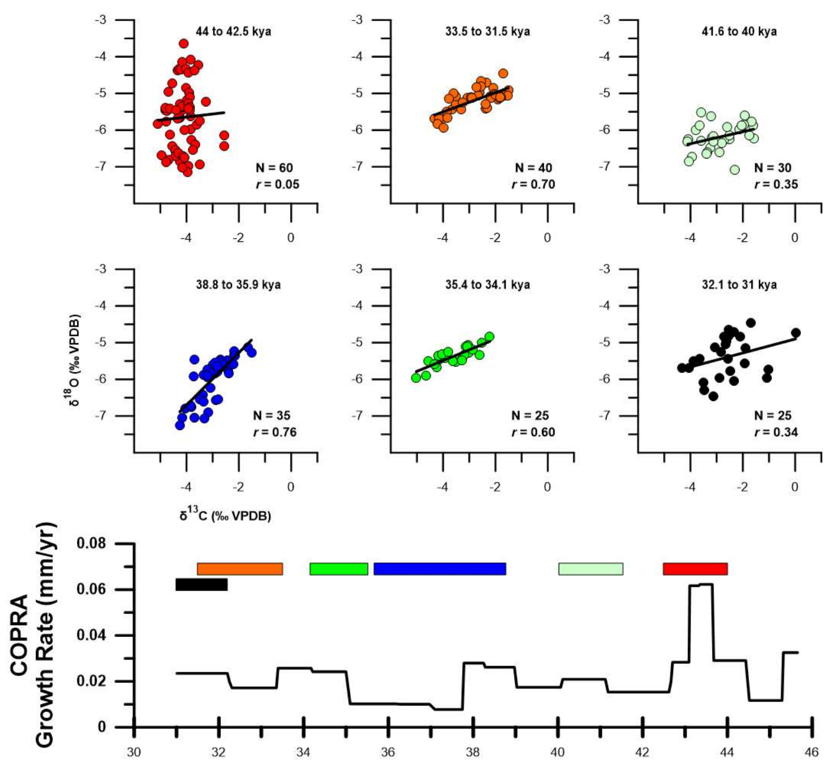

Figure 09: Correlation coefficient sub-analysis of varying periods of time. There are multiple periods after GI-8 (38.5 kya) that show significant positive correlation. These periods are from 38.8-35.9 kya (r = 076, p < 0.001), 35.4-34.1 kya (r = 0.60, p < 0.001), and 33.5-31.5 kya (r = 0.7, p < 0.001). There is poor correlation during the period of relatively fast growth around GI-11 or 43.5 kya (r = 0.05, p = 0.733). Furthermore, correlation does not appear to correspond to growth rate.

Based on the uranium-series chronology, each isotope measurement represents on average, 50 years of growth. Since elemental measurements were done at half the resolution, their resolution averages 100 years per measurement (Fig. 10). Each of the elemental measurements are significantly correlated to one another for the entire time-series, with Ba and Mg showing the greatest correlation ($r = 0.71$, $p < 0.001$). Correlation coefficients between each trace element are shown in fig.11.

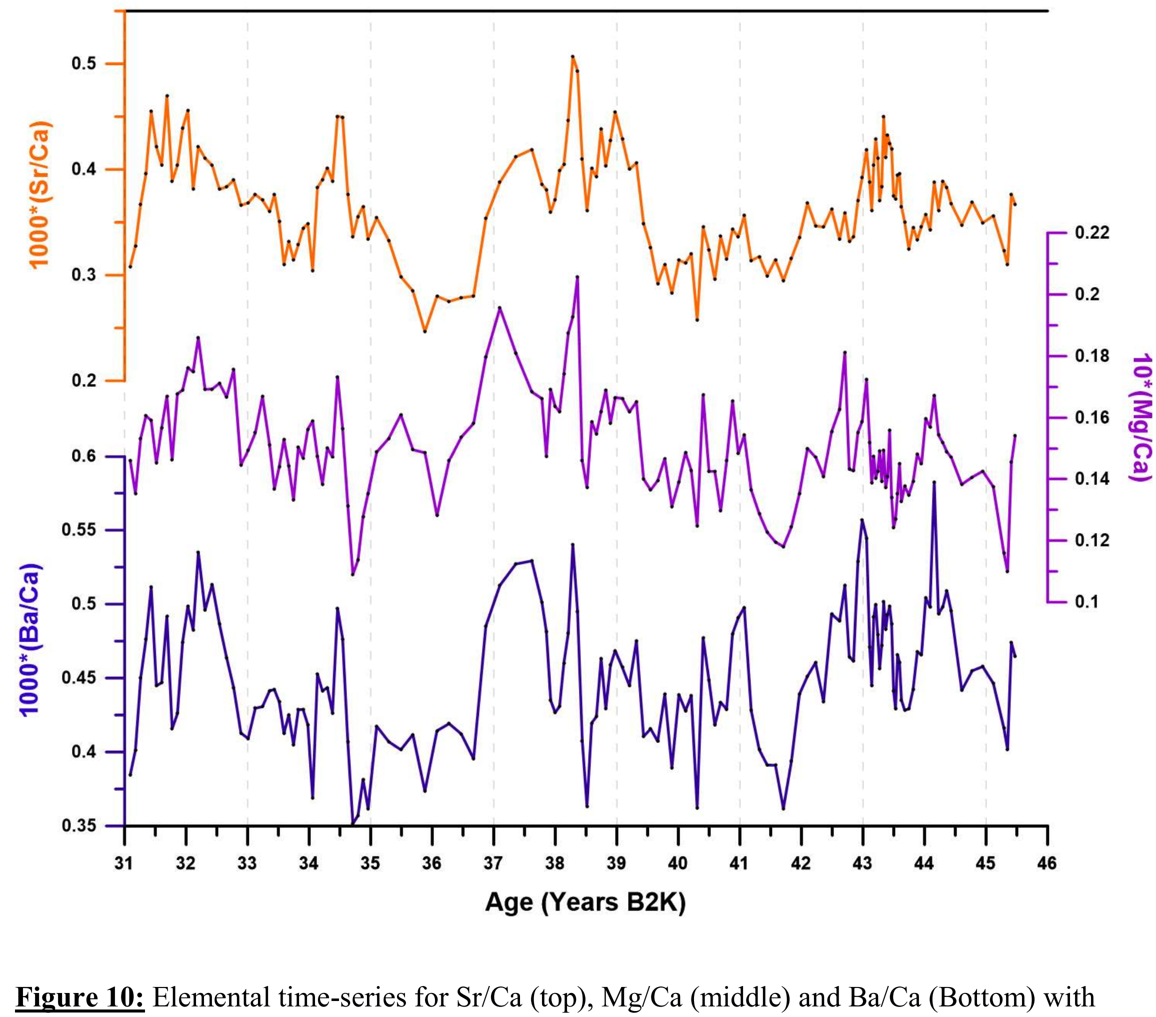

Figure 10: Elemental time-series for Sr/Ca (top), Mg/Ca (middle) and Ba/Ca (Bottom) with each axis reported in parts per million (ppm).

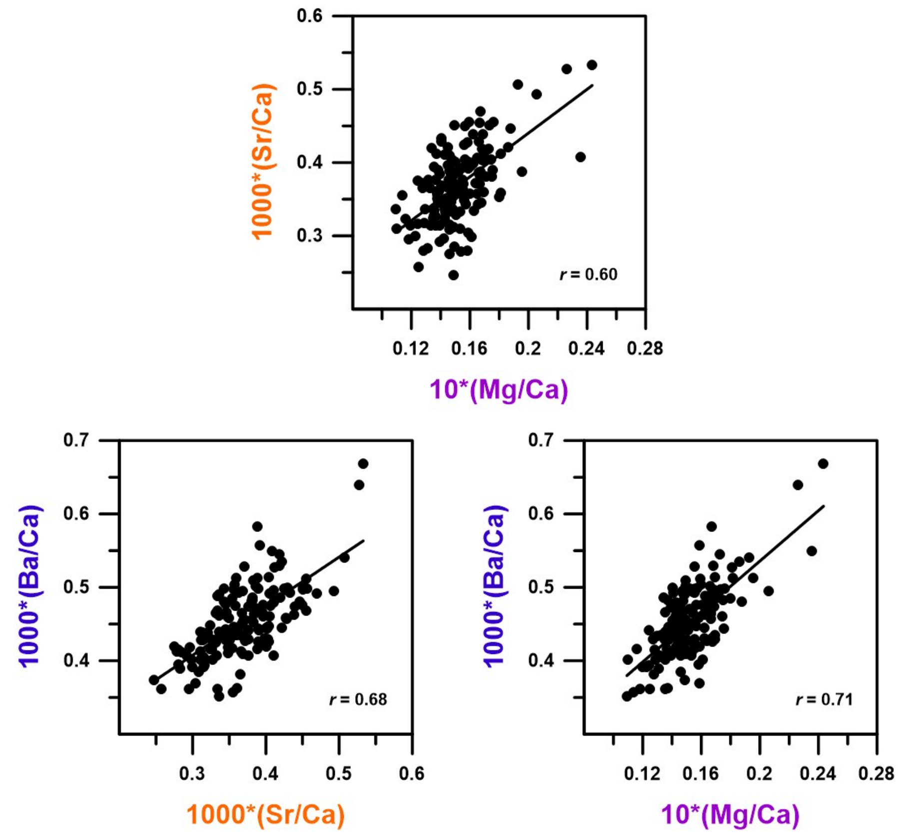

Figure 11: Correlation coefficients between each element, with each axis reported in parts per million (ppm). Mg/Ca-Ba/Ca (r = 0.71, p < 0.001), Ba/Ca-Sr/Ca (r = 0.68, p < 0.001), Sr/Ca-Mg/Ca (r = 0.60, p <0.001)

3.3 – Grayscale and Statistical Analyses

There is a total of 4208 grayscale measurements with each measurement taken over 0.072 mm (Fig. 12). Gray values from reflected light vary from ~140 (darker) to ~230 (lighter). At this resolution, each measurement represents on average, 3.6 years of growth. REDfit periodicities for $\delta^{13}C$, $\delta^{18}O$, Mg/Ca, Sr/Ca, and grayscale are shown in table 03.

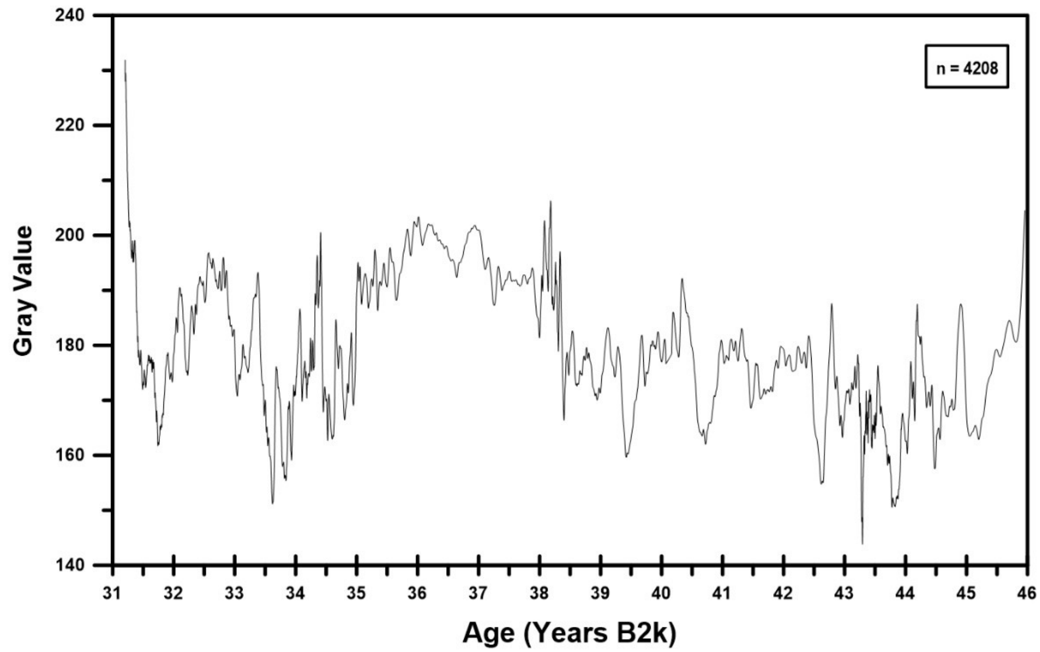

Figure 12: Grayscale time-series for the post-hiatus section.

Table 03: BC-5 REDFIT Periodicities for isotope, elemental, and grayscale measurements (Schulz & Mudelsee 2001)

Time-series	**Confidence Interval**			
	99%	95%	90%	80%
$\delta^{13}C$				1460
$\delta^{18}O$			1122, 972	1825, 1326
Mg/Ca			1475	
Sr/Ca		735		1135
Grayscale	990, 820, 671, 617, 411, 380, 352, 315	781, 493, 302, 290, 231	2469	

CHAPTER IV DICUSSION

4.1 – Comparison to a Modern, Holocene Record

In the BC-11 Holocene record there is significant positive correlation of $\delta^{18}O$ and $\delta^{13}C$, and significant negative correlation of the stable isotopes to growth rate. These characteristics of stable isotope and annual band time series are interpreted as a strong indicator of drought and pluvial episodes, even with a kinetic fractionation effect (Asmerom et al., 2013). In BC-5, $\delta^{18}O$ values are overall lower than those in BC-11 by about -1‰, which would be expected assuming an overall colder climate and greater proportion of isotopically light winter moisture delivery to SWNA (Fig. 13).

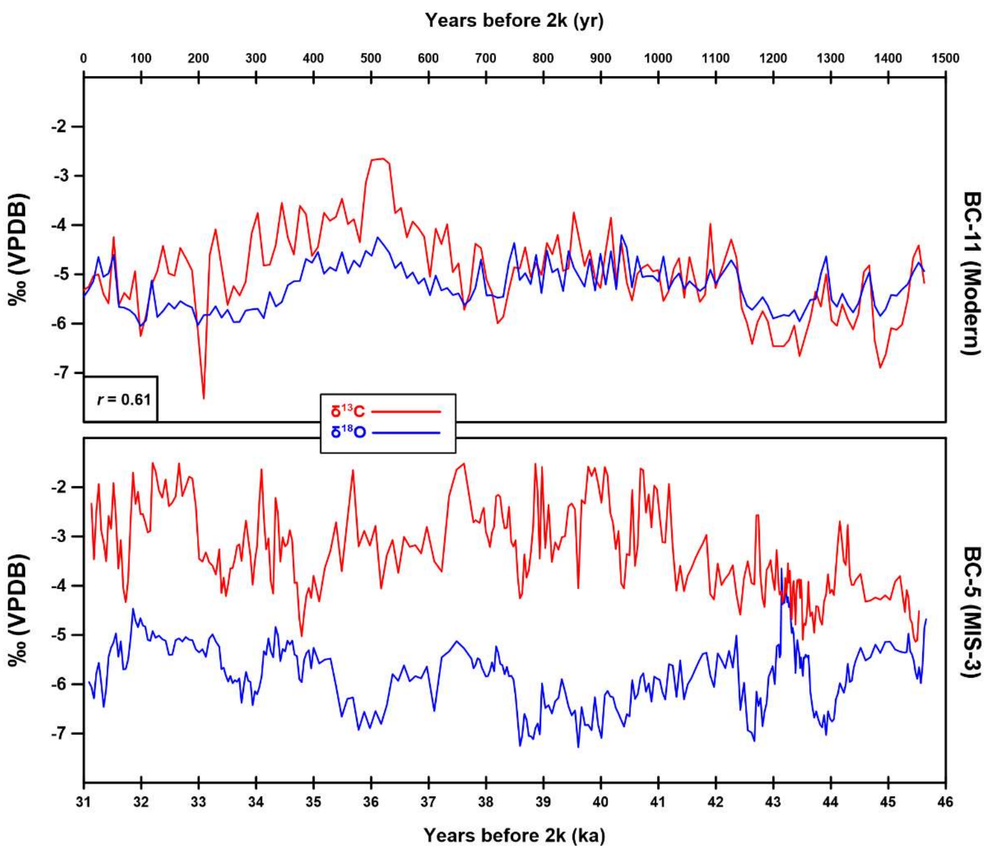

<u>Figure 13:</u> Comparison of BC-11 from Asmerom et al.(2013)(Top) and post-hiatus BC-5 from this study (Bottom). Red = $\delta^{13}C$ and blue = $\delta^{18}O$.

However, $\delta^{13}C$ values are elevated, on average, by +2‰ in comparison to BC-11, and correlation of $\delta^{18}O$ and $\delta^{13}C$ is inconsistent throughout the BC-5 record. One notable difference between the BC-5 and BC-11 stalagmites is the color of the calcite, which may be responsible for the difference in $\delta^{13}C$. BC-5 is a darker yellowish orange, as compared to the relatively light-gray and white color of the calcite in BC-11 (fig. 3). The noticeably darker calcite color seen in BC-5 resembles Holocene speleothems from higher elevations in the Guadalupe Mountains.

At higher elevations, desert vegetation that is typical around Carlsbad Cavern gives way to a more forested environment with greater soil development. The difference in soil development allows for more organic material to be transported to precipitating calcite by infiltrating waters, leading to a darker orange color. Since BC-5 is similar in color to speleothems from the higher elevations, the environment around Carlsbad Cavern can be interpreted as having been similarly forested with greater soil development during MIS-3. Additionally, an effectively wetter climate during MIS-3 is necessary to explain the presence of pluvial lakes in SWNA (Allen & Anderson 2000), which likely allowed for greater vegetation growth. Greater amounts of vegetation and soil productivity should then drive more negative $\delta^{13}C$ values, since there would be a greater amount of isotopically light organic carbon available for cave drip waters. However, we see a 2‰ decrease from the late Pleistocene BC-5 to Holocene BC-11 record, even though BC-5 should represent a relatively wet period in comparison to the modern BC-11 record, indicating that other environmental variables are controlling $\delta^{13}C$.

Another scenario is that greater soil development during MIS-3 allowed for longer residence times of infiltrating waters in the epikarst as compared to the modern environment where soil development is minimal (Li et al., 2014). Cooler water having greater *p*CO2 due to cooler climate and more vegetation could increase the interaction of infiltrating waters with bedrock, which results in greater bedrock dissolution (Faulkner 2006). Bedrock measurements average between 3-8‰ in the Carlsbad Cavern area (Hill, 1996), and increasing the amount of bedrock carbon in cave dripwaters would result in a positive $\delta^{13}C$ shift that may not be representative of a change in vegetation. However, determining the degree to which bedrock contributed to the $\delta^{13}C$ of speleothem calcite is difficult, and requires speleothem calcite elemental measurements, which are a better indicator of water-bedrock interaction.

The +2‰ difference could also be a result of lower atmospheric pCO_2 during the last glacial period (Wong & Breecker 2015; Breecker 2017). Wong & Breecker (2015) suggest a maximum 2‰ $\delta^{13}C$ difference between last glacial and Holocene speleothem records based on previous studies that propose a strong atmospheric pCO_2 control on the $\delta^{13}C$ of C_3 plants (Schubert & Jahren, 2012), and in turn, a control on speleothem $\delta^{13}C$. However, the belowground processes controlling $\delta^{13}C$ are complex, and for single speleothem records it is difficult to ignore other processes (Breecker 2017), especially in the evaporative and well-ventilated cave environment where BC-5 grew. Regardless, the noticeable 2‰ difference between the BC-5 $\delta^{13}C$ record and BC-11 $\delta^{13}C$ record is a strong indication of a difference in environmental variables and to a certain extent, could be attributed to lower atmospheric pCO_2 during the last glacial.

Overall, there are noticeable similarities and differences between BC-5 and the 1500-year modern BC-11 record that may indicate specific climates and define environmental variables such as vegetation, soil development, degree of bedrock dissolution, and an influence of atmospheric pCO_2. However, the relatively short BC-11 record and the much longer ~15 ky BC-5 makes a true comparison difficult. To further understand the much longer ~15 ky BC-5 record, a comparison to longer-lived records such as FS-2 and COB is needed.

4.2 – Evidence for GS and GI events from stable isotopes and other regional records

The BC-5 $\delta^{18}O$ record shows noticeable millennial-scale shifts, that match the timing and duration of GI's and GS's in the NGRIP record from Rasmussen et al. (2014) (Fig. 14). GI-12, GI-11, and GI-10 are clearly expressed in the BC-5 $\delta^{18}O$ record. However, following the positive shift in $\delta^{18}O$ to GI-10, there is a gradual decline in $\delta^{18}O$ from 42-38.5 kya, and GI-9 is not clearly seen in the record.

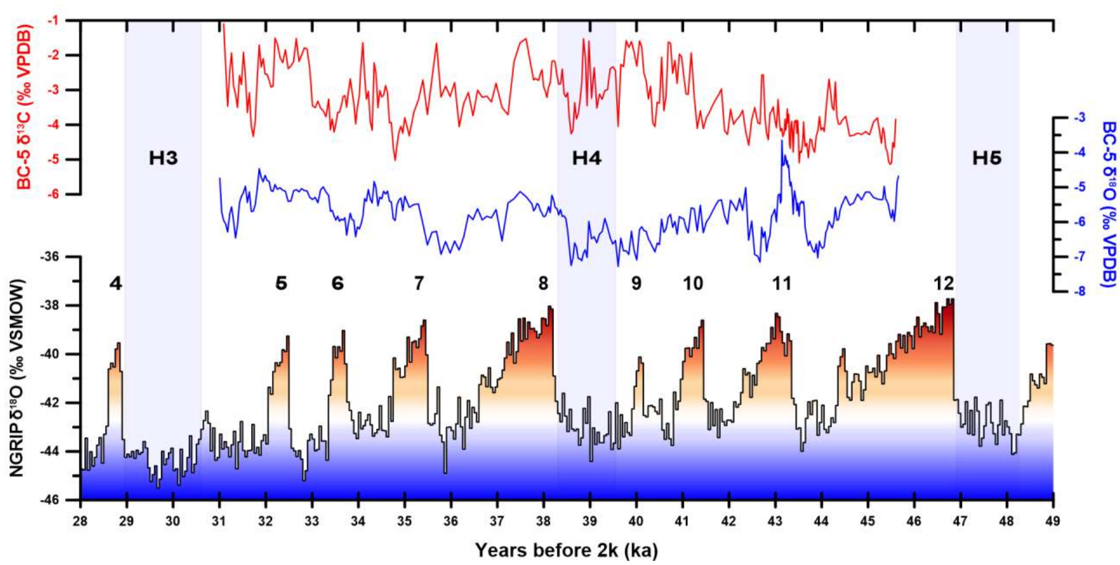

Figure 14: Comparison of $\delta^{18}O$ in BC-5 to the $\delta^{18}O$ NGRIP record. Glacial interstadials (GI) are marked from 4-12 and Heinrich events 3, 4 and 5 according to Rasmussen et al. (2014).

Heinrich event 4 (GS-9) then coincides with the lowest $\delta^{18}O$ values in BC-5, with the lowest value of -7.25‰ preceding the roughly +2‰ shift to GI-8. GI-7 then seems to be shown in BC-5, but GI-6 and GI-5 are not as apparent.

In comparing BC-5 to the FS-2 and COB records, we see a strong similarity between each of the $\delta^{18}O$ records (Fig. 15). Like the comparison of NGRIP to BC-5, GI-12, GI-11, GI-10, GI-8, and GI-7 match in timing and duration between each of the SWNA speleothem records, with no clear match for GI-9, GI-6, and GI-5.

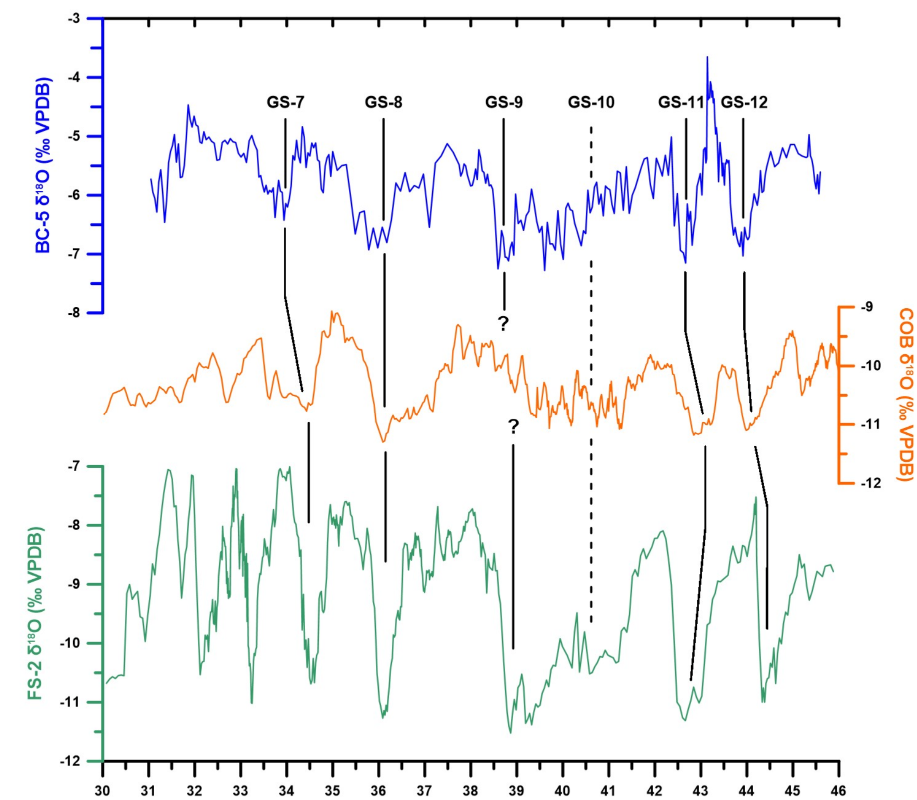

Figure 15: $\delta^{18}O$ records from BC-5, COB (Wagner et al., 2010), and FS-2 (Asmerom et al., 2010). BC-5 is at the top (blue), COB is in the middle (orange), and FS-2 is at the bottom (green).

The GI-9, GI-6, and GI-5 interstadials are relatively short-lived compared to the other interstadials in the NGRIP record and may have not had a significant enough impact on

SWNA climate to be reflected in speleothem records. Regardless, the clear match of the other interstadials between three different SWNA speleothem records offers credibility to the well-supported hypothesis of a shifting westerly storm track in response to DO-events. Furthermore, this suggest that the BC-5 $\delta^{18}O$ record, like COB and FS-2, is a record of SWNA moisture source variability, even though BC-5 grew in a cave environment that is susceptible to kinetic fractionation effects.

Where the BC-5 $\delta^{18}O$ record clearly matches NGRIP and other speleothem records, the BC-5 $\delta^{13}C$ record is more complex, and does not show a clear response to DO-events. Also, the carbon record is far noisier than $\delta^{18}O$, and has centennial shifts of 2-3‰. These shifts may be more representative of changes in local climate conditions, such as effective moisture and vegetation, as opposed to the $\delta^{18}O$ moisture source record. As previously discussed, the heavy $\delta^{13}C$ values of BC-5 relative to the Holocene BC-11 record seemed to indicate an atmospheric $p\mathrm{CO_2}$ control on the $\delta^{13}C$ of vegetation, and subsequently, on speleothem $\delta^{13}C$ values (Breecker, 2017). $\delta^{13}C$ should then be a strong reflection of vegetation, and positive correlation between carbon and oxygen could be an indication of changes in effective moisture in response to the shifting westerly storm track or DO-events.

The shift from the H4 stadial (GS-9) to a relatively long-lived interstadial (GI-8) seen in NGRIP is concurrent with a shift to heavier $\delta^{18}O$ values in BC-5 from 38.5-35.5 kya. GI-8 lasted from 38.2-36.58 kya in the NGRIP record (Rasmussen et al., 2014), and age uncertainties between the two records allow for these two periods to overlap. As the westerly storm track shifted north in response to hemispheric warming due to the DO-event, less winter moisture was delivered to SWNA and in turn, correlation between $\delta^{18}O$

and $\delta^{13}C$ becomes significant ($r = 0.78$, $p < 0.001$) from 38.5-35.5 kya. The shift to positive correlation and heavier $\delta^{13}C$ values suggests a decrease in vegetation and soil productivity, or an increase in residence times and water-bedrock interaction (Lachniet, 2009; Polyak et al., 2012). The GS-9 to GI-8 transition then seems to represent a change from relatively wet to arid conditions, which resulted from a decrease in winter moisture delivery to SWNA.

A $\delta^{18}O$ speleothem record from China documents that GS-9 lasted from 39.7-38.3 kya (Zhou et al., 2014), with the end of GS-9 only 200 years and within error of the end of GS-9 in the BC-5 record. A record from Lake Manix in southern California also suggest a termination of a major lake high-stand coincident with the GS-9 to GI-8 transition (Reheis et al., 2014). The termination of the lake high-stand supports the interpretation that positive correlation between the isotope records in BC-5 during the GS-9 to GI-8 transition is an indication of a decrease in effective moisture for SWNA. During GS-9, correlation of $\delta^{18}O$ and $\delta^{13}C$ is poor, but $\delta^{13}C$ values are still relatively heavy in comparison to the rest of the record, with values like what are seen during GI-8. The heavy values may indicate that a higher proportion of winter moisture during what is assumed to be a relatively wet period in SWNA is not the dominant control on $\delta^{13}C$. Instead, $\delta^{13}C$ may be more influenced by degassing rates on cave drip waters during stadials, which would have little impact on $\delta^{18}O$. Assuming stadials are relatively cold in comparison to interstadials in SWNA, colder temperatures would promote greater cave ventilation, which would lower cave air $p\mathrm{CO_2}$ and increase degassing rates. In addition, colder infiltrating waters having higher pCO2 from thicker vegetation would contribute to greater water/bedrock interaction.

At 43.5 kya in BC-5, the nearly +3‰ shift in $\delta^{18}O$ coeval with GI-11 is the largest shift occurring in the record and lasts for approximately 1500 years. This GI-11 peak is also present in the FS-2, and COB records, and they are all similar in duration. The GS-10 and GS-11 troughs also match nicely between each of the records. However, unlike the GS-9 to GI-8 transition, $\delta^{13}C$ is not clearly connected to these events, and does not covary with $\delta^{18}O$. $\delta^{13}C$ is also at the lowest values seen in the record from 46-42 kya, with values close to -5‰, and U-series ages suggest that growth rate is at its highest during GI-11 (Table 1 and Fig. 7), indicating that conditions for calcite precipitation were greatest. The apparent disconnect between $\delta^{13}C$ and $\delta^{18}O$ in the early part of the record, 46-42 kya, may indicate that DO-events were not having a significant impact on effective moisture in the region. Therefore, DO-events did not have a consistent impact on effective moisture for SWNA, since clear positive correlation is seen after H4.

Further comparison of the BC-5 $\delta^{13}C$ record, when tuned to a speleothem $\delta^{18}O$ Asian monsoon record (Cheng et al., 2017), shows an inverse relationship (Fig. 16), like what was reported between the FS-2 $\delta^{18}O$ and Hulu $\delta^{18}O$ Asian monsoon record in Asmerom et al., 2010. The inverse relationship between the speleothem $\delta^{18}O$ records was interpreted as a reflection of the polar jets movement in response to DO-events. The inverse relationship between BC-5 $\delta^{13}C$ and the Asian monsoon record supports the interpretation that effective moisture was impacted to some degree in SWNA by DO-events and Heinrich events, assuming $\delta^{13}C$ reflects effective moisture to some extent.

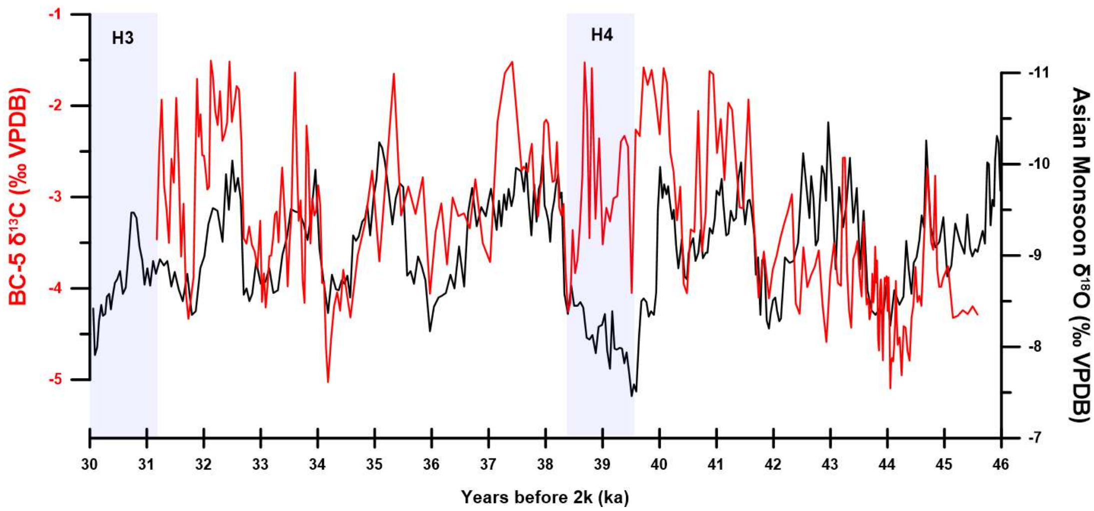

<u>Figure 16</u>: The tuned BC-5 carbon record in comparison to the Asian Monsoon oxygen record from Cheng et al., 2017. The BC-5 carbon record was tuned to more clearly match by using the method described in Asmerom et al., 2017, and is further described in the Appendix. Note that the Asian Monsoon record y-axis is inverted in comparison to the BC-5 y-axis Troughs represent relatively wet periods, and peaks represent dry periods in response to DO-events and changes in winter moisture delivery. Heinrich events are highlighted with blue bars.

Since the relationship is inverse, increases in winter moisture delivery during stadials resulted in a relatively wet climate in SWNA, whereas a stadial in Southeast Asia corresponds to a dry climate, and vice versa for interstadials. However, the correlation between the two records isn't consistent, indicating that the changes in effective moisture are not dramatic, but do occur to some extent. The fact that a relationship can be seen between the two proxies, despite the dynamic cave environment where BC-5 grew, is further evidence of the teleconnection and changes in effective moisture that can be attributed to DO-events.

Greater precipitation amounts during GI-11 were reported for Lake Bonneville in the Great Basin that seemingly conflict with the shifting westerly storm track hypothesis

(Nishizawa et al., 2013). While this would be an important finding, Oviatt et al. (2014) show that lake chronologies for this time are difficult to obtain, and that their ^{14}C chronology, based heavily on dating of carbonate, is near the limit of that technique and problematic. While there is another important paper opposing the westerly storm track hypothesis during the LGM (Lyle et al., 2012), Lachniet et al. (2014) make a stronger case for a high latitude source of moisture filling lakes, not tropical input. The lack of covariance between $\delta^{13}C$ and $\delta^{18}O$ from 46 to 38.5 kya supports a period within this entire record when calcite was precipitated in near equilibrium with cave waters. Conditions in Bat Cave passage during the early part of the record, whatever they were, were most conducive to calcite precipitation and equilibrium fractionation, which allowed for DO-events to be clearly expressed in the $\delta^{18}O$ record.

After the transition from GS-9 to GI-8 in the BC-5 record there is a positive trend in $\delta^{18}O$ towards the end of growth, which is punctuated by broad, millennial peaks in $\delta^{18}O$. The positive trend may represent a gradual decrease in winter moisture delivery to the region, leading to the end of growth, which coincides with Heinrich event 3 (H3). From 36-31 kya there are two peaks in $\delta^{18}O$ that appear to correspond to GI-7, GI-6, or GI-5 in NGRIP. At 35.5 kya, BC-5 $\delta^{18}O$ shifts by about +1.5‰, and seems to correspond to the GS-8 to GI-7 transition in NGRIP. However, BC-5 $\delta^{18}O$ values stay elevated till 34 kya for 1.5 ky's, whereas GI-7 in NGRIP only lasts for about 740 years (Rasmussen et al., 2014). In each of the SWNA speleothem records, GI-7, GI-6, and GI-5 are not clearly connected, and the timing and duration of each event is not coherent. The latter part of the BC-5 record, and other SWNA records, seems to suggest that DO-events became less controlling on SWNA climate, up to the point where both the COB and BC-5 stalagmites stop growing, before H3.

It is the well-ventilated evaporative cave environment from which BC-5 grew that is altering the stable isotope signal, and therefore important to take into consideration ventilation effects when comparing BC-5 to NGRIP, FS-2 and COB. Ventilation mechanics would have changed in Bat Cave Passage from glacial to modern times, and likely during stadials and interstadials. Of course, this depends on the degree to which regional temperatures and effective moisture changed, which remains largely unknown. A comprehensive study of cave ventilation showed that in general, speleothems grow more during the cool season and less during the warm season in temperate to boreal regions (James et al., 2015). If average-annual temperatures in SWNA decreased during stadials, then Batcave Passage should have ventilated more and lead to a speleothem record more dominated by the isotopic composition of winter precipitation (Wong et al., 2015). This interpretation also dictates that speleothem growth is favored during periods of enhanced ventilation, when the difference between cave air $p\mathrm{CO_2}$ and drip water $p\mathrm{CO_2}$ is at its greatest (Banner et al., 2007). However, for Carlsbad Cavern this difference is greatest during the winter and early spring, but drip rates in Carlsbad Cavern were significantly less during the winter, and one drip site stopped dripping altogether (Rasmussen, 2006).

Stalagmite BC-11 has a far higher growth rate than BC-5, and $\delta^{13}C$ values are still lower, which seems to suggest that degassing rates and increased calcite precipitation were not an important control on $\delta^{13}C$ in BC-5. Therefore, growth rate and $\delta^{13}C$ would seem less reliable as a proxy for greater precipitation in this case. It shows that these types of interpretations are difficult to apply for studies of well-ventilated cave environments, where ventilation effects, such as changes in degassing rates, may be a strong control on carbon isotope fractionation. Determining whether increased ventilation in response to colder temperatures or a decrease in effective moisture would dominate the $\delta^{13}C$ speleothem record is difficult to quantify based on isotopes alone and requires an elemental record to further discuss. Regardless, the BC-5 $\delta^{18}O$ record further supports the shifting westerly storm track hypothesis, as has been proposed in previous SWNA speleothem research. Furthermore, the relatively light $\delta^{13}C$ values at the beginning of the record, and gradual shift to heavier values towards the end of the record, seem to suggest a gradual decrease in effective moisture up to end of growth.

4.3 - Elemental time-series as a record of effective moisture

There is significant positive correlation between Mg/Ca, Ba/Ca, and Sr/Ca ($r > 0.6$, $p < 0.001$) for the entirety of the BC-5 record. The strong relationship between each element for 15,000 years is an indication that they were controlled by similar karst processes, such as water-bedrock interaction or prior calcite precipitation (PCP), rather than partition coefficients connected to temperature (Fairchild et al., 2000; Fairchild & Treble 2009; Oster et al., 2012). A comparison of the isotope and elemental time-series shows clear, extended periods of covariation (Fig. 17). Notable covariance is seen between $\delta^{18}O$ and Sr/Ca, which has been observed in other late Pleistocene speleothem records (Cruz et al., 2007). This relationship in BC-5 suggests that, as in Cruz et al.

(2007), changes in effective moisture were concurrent with changes in the delivery of isotopically light winter moisture to SWNA, with the assumption that $\delta^{18}O$ is primarily a moisture source record and that Sr/Ca is an effective moisture record.

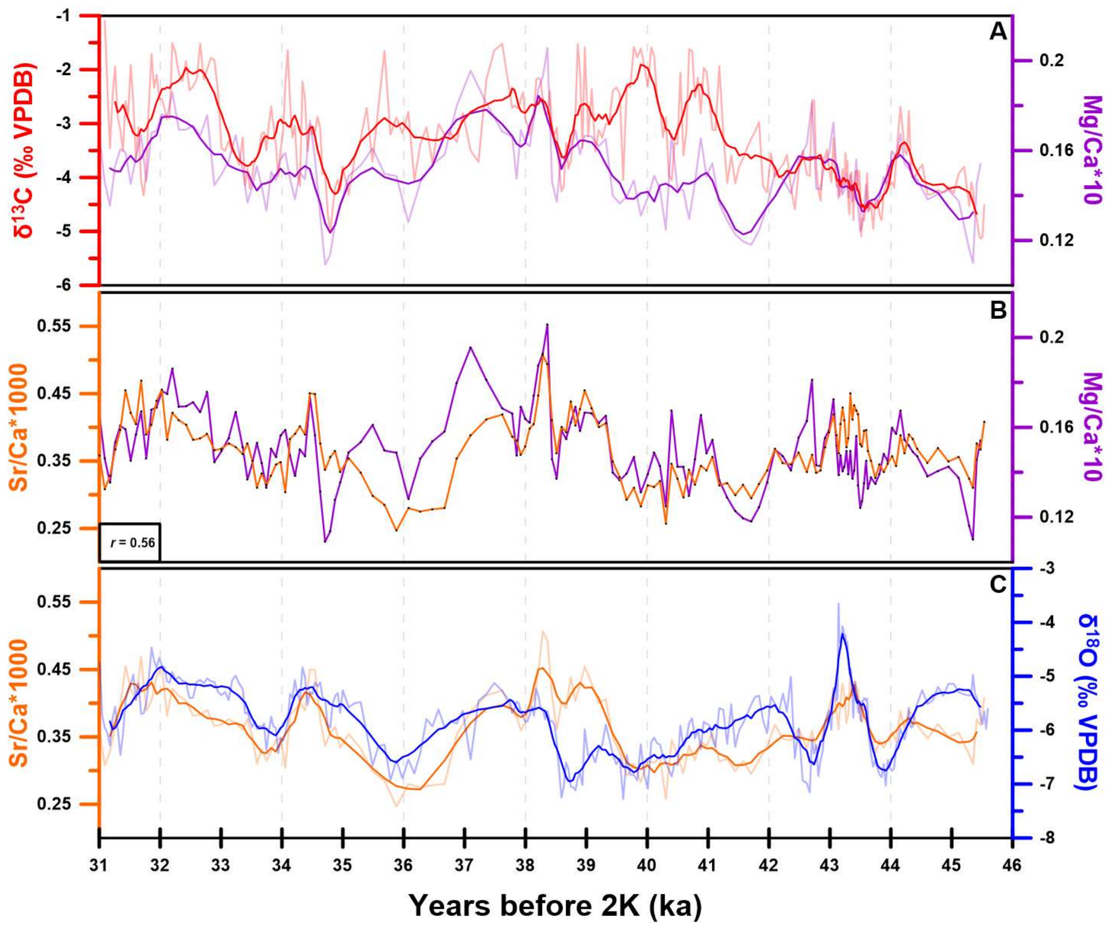

Figure 17: A comparison of the elemental and isotope measurements for the post-hiatus period. The top box contains $\delta^{13}C$ (red) and Mg/Ca (purple), Mg/Ca and Sr/Ca (orange) in the middle ($r = 0.56$, $p < 0.001$), and $\delta^{18}O$ (blue) and Sr/Ca on the bottom. For the top and bottom boxes, the actual measurements are transparent, and there is a running average on top of the values. For the stable isotopes, it is a 7-point running average, and a 3-point running average for the elemental.

The BC-5 isotope records suggest that the transition from GS-9 to GI-8, at 38.5 kya, resulted in a decrease in effective moisture in SWNA. At the same time, there is an increase in Sr/Ca and Mg/Ca, which supports the stable isotope interpretation. The largest values of Sr/Ca and Mg/Ca are also seen during GI-8, with a prominent peak centered around 38.25 kya (Fig. 17).

An increase in elemental ratios is thought to be a result of an increase in water-bedrock interaction as effective moisture decreases, which results in a greater amount of Sr or Mg in drip-waters as greater bedrock dissolution occurs. The increase in elemental ratios is also attributed to an increase in Prior Calcite Precipitation (PCP), since drip rates slow in response to a decrease in effective moisture, which promotes PCP in the epikarst and cave environment (Fairchild & Treble 2009). Therefore, the clear covariation between each of the isotopes and elemental ratios after H4 seems to suggest that a severe drought in SWNA followed or was triggered by the event, as evidenced by the pronounced covariation and positive shift in each proxy (Fig. 17).

Like the $\delta^{18}O$ and Sr/Ca relationship, Mg/Ca and $\delta^{13}C$ covary throughout the record. However, there are extended periods where covariation is not apparent, most notably from 42-38 kya. Typical speleothem records show strong correlation between Mg/Ca and $\delta^{13}C$ and use this as an indication that elemental and isotopic records were primarily controlled by water-bedrock interactions and PCP (Johnson et al., 2006). Since this is not the case from 42-37 kya, the $\delta^{13}C$ record was likely controlled by processes separate from those controlling elemental concentrations. $\delta^{13}C$ may have been more sensitive to atmospheric $p\mathrm{CO_2}$, ventilation, or soil processes from 42-37 kya, as has been previously suggested in this study and other speleothem records (Cruz et al., 2007; Oster et al., 2012). A gradual increase in $\delta^{13}C$ from the lowest values of -5‰ at the beginning of growth, to -2‰ near H4 could be an indication of a drying trend if there was notable covariance with Mg/Ca. However, a gradual increase in Mg/Ca over the same time is not as clear, further supporting the interpretation that $\delta^{13}C$ is more than an effective moisture record. However, from 46-42 kya, Mg/Ca and $\delta^{13}C$ clearly co-vary, and support the interpretation that the early part of this record behaved more like a system in isotopic equilibrium typical of other speleothem records, where $\delta^{13}C$ acted as an effective moisture record.

The clear covariation of Mg/Ca and $\delta^{13}C$ during 46-42 kya seems to suggest as Johnson et al. (2006) have reported, that PCP and increased water-bedrock interaction drives the covariance between the two. This is evidence that from 46 to 42 ka, DO-events were not a dominant control on effective moisture in SWNA, since $\delta^{13}C$ and Mg/Ca do not covary with $\delta^{18}O$ in BC-5. Another possible interpretation is that Mg/Ca and $\delta^{13}C$, in comparison to $\delta^{18}O$, are too easily influenced by local climate conditions and karst processes and are decoupled from regional changes in moisture source. Focusing on GI-11, the disconnect between Mg/Ca and $\delta^{13}C$ with $\delta^{18}O$ offers a more robust interpretation that the isotope and element proxies are tied to climate. $\delta^{18}O$ clearly shows moisture source, and Mg/Ca and $\delta^{13}C$ either reflect local climate conditions or a lack of change in effective moisture. Therefore, the largest $\delta^{18}O$ peak in BC-5 during GI-11 does not seem to correspond to a decrease in effective moisture. If anything, the early part of the record, from 46-42 kya, represents the wettest period, since Mg/Ca and $\delta^{13}C$ values are at their lowest and covary.

The BC-5 $\delta^{18}O$ record is clearly tied to moisture source and other speleothem records from SWNA, which are tied to the NGRIP record, and document DO-events. DO-events impacted karst mechanics to such an extent that the Sr/Ca ratio of the speleothem calcite covaried with $\delta^{18}O$, even though Mg/Ca and $\delta^{13}C$ seem to suggest that changes in moisture source do not correspond to immediate changes in effective moisture. Steponaitus et al. 2015 suggest that Sr/Ca has reduced sensitivity to PCP, since the partition coefficient is a magnitude less than the Mg/Ca partition coefficient, which are D_{Mg} (0.0125) and D_{Sr} (0.125) as calculated from Day and Henderson (2013). While there is strong correlation between Sr/Ca and Mg/Ca ($r = 0.56$, $p < 0.001$), indicating some degree of water-bedrock interaction and PCP control, there must be an additional mechanism that is coupling Sr/Ca to $\delta^{18}O$. One possibility is an influx of Sr rich aeolian dust as moisture source changes, which has been documented in other speleothem studies using Sr isotopes (Li et al., 2005; Orland et al., 2014). Further study into Sr isotopes could reveal whether there were influxes of aeolian dust in response to a shifting polar jet. The sensitivity of $\delta^{18}O$ and Sr/Ca to temperature during calcite precipitation could also be coupling the two systems, but the strong correlation of Sr/Ca with Mg/Ca and Ba/Ca seems to suggest otherwise. Overall, the comparison of the isotope and elemental proxies in BC-5 show a complex climate history, where karst mechanisms and the dominant controls on elemental ratios changed in response to changes in the regional climate.

4.4 – Comparison of grayscale and spectral analyses to the elemental and isotope time-series

Grayscale of stalagmite BC-5 is a record of growth changes. Unfortunately, they are not easily tied to specific climate events beyond qualitative shifts. However, lower values should represent darker calcite, and in this sample darker calcite is caused by greater amounts of organic components making the sample yellowish orange when compared to Holocene samples. More yellowish orange, the more organic content, and the darker the gray values. As such, the grayscale can to some degree represent changes in growth likely tied to climate change events. Therefore, the grayscale yields climatic periodicities linked to changes in growth, and likely indicate general changes in climate. More importantly, the resolution of grayscale time series shows important climate periodicities at a level not allowable using elements and stable isotopes. REDFIT analysis of grayscale shows multiple, centennial-scale, periodicities between 300-1000 years. These periodicities could be an expression of GI's and GS's. However, the grayscale periodicities do not match the $\delta^{18}O$, $\delta^{13}C$, Sr/Ca or Mg/Ca periodicities which, are millennial in scale. This could be a result of the difference in resolution between the time-series. A comparison of all the time-series, including the grayscale, shows the clear connection between each proxy at 38.5 kya, and the apparent disconnect between some proxies at 43.5 kya (Fig. 18).

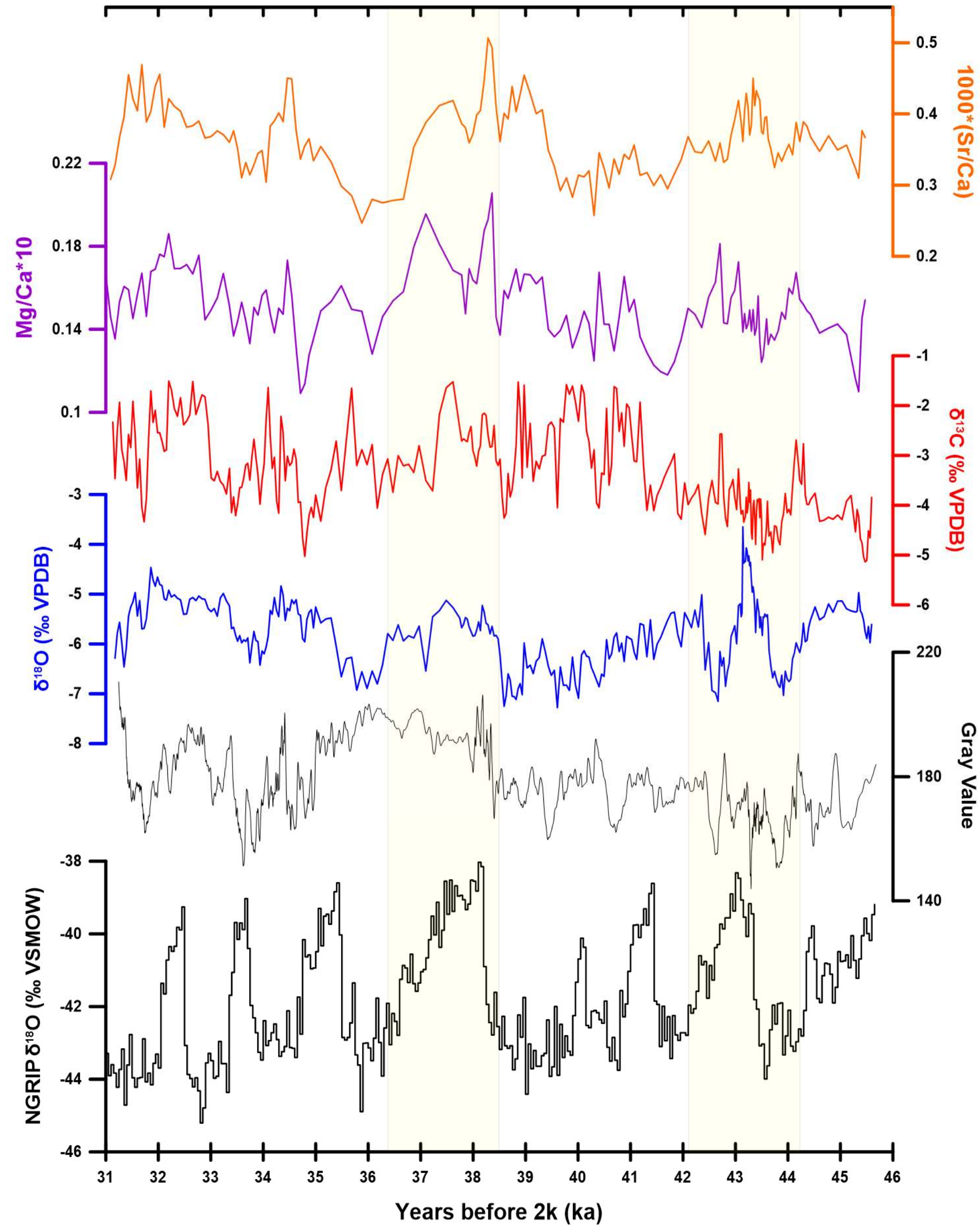

Figure 18: Elemental, isotope, and grayscale time-series for BC-5 and the NGRIP record. Yellow bars highlight periods where the records show similar changes.

Dark gray (lower values) for the lower part of the sample seems to indicate that climate was conducive to allowing more organic compounds into the calcite fabric, giving the stalagmite a more yellowish orange color at the bottom than at the top. This type of interpretation would indicate that the period between 38.5 and 34 ka is the period least conducive to accumulation or preservation of organic compounds into the calcite fabric. More specifically, there is a positive shift in grayscale at 38.5 kya during the transition from GS-9 to GI-8, reflecting a decrease in effective moisture over that shift. The absence of shifts to lower values during the stadials and higher values during interstadials, and the overall difference between NGRIP and grayscale, supports the idea that the record was heavily influenced by local climate and karst processes.

CHAPTER V CONCLUSION

The BC-5 stalagmite record from Carlsbad Cavern grew during the latter half of MIS-3 from 46-31 kya. The BC-5 $\delta^{18}O$ time series shows noticeable relationships with the NGRIP, FS-2 and COB time series, in addition to other paleoclimate proxies. During the first half of the record from 46-38 kya, the $\delta^{18}O$ time-series clearly shows GS's and GI's. A clear match of each of the SWNA stalagmite records from 46-38 kya further strengthens the theory of a shifting westerly storm-track in response to GS's and GI's during MIS-3. The expression of DO-events in $\delta^{18}O$ following H4, or GI-8, in BC-5 then becomes less apparent. This is interpreted to be the result of kinetic fractionation effects or local climate conditions that are filtering out or interfering with teleconnections, as is evidenced by an increase in correlation between $\delta^{13}C$ and $\delta^{18}O$ from 38.5 kya to the end of growth.

The $\delta^{13}C$ time-series is more complex than the $\delta^{18}O$ record, and inconsistently correlates with $\delta^{18}O$. For instance, there is no correlation between $\delta^{13}C$ and the largest shift in $\delta^{18}O$ during GI-11, indicating that the two isotope systems were decoupled for the early part of the record. However, one key event at 38.5 kya seems to indicate that the transition from GS-9 to GI-8 resulted in a decrease in effective moisture for SWNA, since both isotopes display an abrupt positive shift in values and strong positive correlation that lasted for a few thousand years. Comparison of the $\delta^{13}C$ time-series to an Asian monsoon $\delta^{18}O$ record shows an inverse relationship. Indicating that changes in the westerly storm-track resulted in changes in effective moisture for SWNA, with stadials representing relatively wet climates in comparison to interstadials.

In comparison to a late Holocene speleothem from Bat Cave passage (BC-11), the MIS-3 late Pleistocene BC-5 $\delta^{13}C$ values are on average, heavier than the Late Holocene BC-11 $\delta^{13}C$ values by 2‰. The darker yellowish orange color of stalagmite BC-5 in comparison to the lighter-grey of BC-11 seems to indicate more soil-related input. Greater vegetation on the surface that would then indicate overall greater effective moisture during the late Pleistocene compared to the Holocene. Yet the expected lighter $\delta^{13}C$ values that reflect greater C3 vegetation growth and soil productivity are not represented in BC-5. Instead, the glacial BC-5 record exhibits heavier values than the Holocene BC-11 record. This difference may be explained by less atmospheric pCO_2 during the last glacial, which promoted heavier $\delta^{13}C$ values for C3 vegetation, and in turn, heavier values for speleothem calcite. Colder infiltrating water may have also interacted with the bedrock, producing heavier $\delta^{13}C$ values.

Elemental measurements confirm some of the findings of the stable isotope interpretations. Mg/Ca and $\delta^{13}C$ clearly show positive covariance from 46-42 kya, which is expected in a well-behaved system where the calcite is precipitating under equilibrium conditions. Mg/Ca and $\delta^{13}C$ are commonly interpreted as records of effective moisture, and further strengthens the Asian monsoon comparison. Another scenario is that Mg/Ca and $\delta^{13}C$ are more reflective of local karst processes, where teleconnections have been filtered out. However, after H4 there is a sharp positive shift in each of the elemental and isotope time-series, suggesting a significant decrease in effective moisture in response to the event. Looking at Sr/Ca, we see that it covaries with $\delta^{18}O$ for most of the record, which also suggests that DO-events effected karst processes to some extent. The difference in partition coefficients between Sr/Ca and Mg/Ca may make Sr/Ca less susceptible to PCP, meaning Sr/Ca may be more sensitive to changes in effective moisture than Mg/Ca and $\delta^{13}C$.

Spectral analyses of different proxies show a mix of possibly important periodicities. The expected 1450-year periodicity that is thought to represent DO-events shows up only in the $\delta^{13}C$ and Mg/Ca time series, but not in the $\delta^{18}O$ time-series, which clearly matches other records. Overall, the multiproxy BC-5 stalagmite record supports the shifting westerly storm track hypothesis, but the $\delta^{13}C$ time-series is more difficult to interpret and may be more of a local effective moisture record. Comparison to the elemental time-series further strengthens stable isotope interpretations, and noticeable relationships that have been reported in other speleothem studies are apparent in BC-5. Therefore, the multi-proxy BC-5 record suggests a complex climate history in SWNA and highlights the difficulty in interpreting elemental and isotope time-series in a dynamic cave environment during a period of pronounced climate variability.

REFERENCES

D. K. Adams, A. C. Comrie, The north American monsoon. *Bulletin of the American Meteorological Society* **78**, 2197-2213 (1997).

B. D. Allen, R. Y. Anderson, Evidence from Western north america for rapid shifts in climate during the last glacial maximum. *Science (New York, N.Y.)* **260**, 1920-1923 (1993).

E. Antevs, Geologic-Climatic Dating in the West. *American Antiquity* **20**, 317-335 (1955).

K. Arpe, S. a. G. Leroy, U. Mikolajewicz, A comparison of climate simulations for the last glacial maximum with three different versions of the ECHAM model and implications for summer-green tree refugia. (2011).

Y. Asmerom, V. Polyak, J. Schwieters, C. Bouman, Routine high-precision U–Th isotope analyses for paleoclimate chronology. *Geochimica et Cosmochimica Acta* **70**, A24 (2006).

Y. Asmerom, V. J. Polyak, S. J. Burns, Variable winter moisture in the southwestern United States linked to rapid glacial climate shifts. *Nature Geoscience* **3**, 114-117 (2010).

Y. Asmerom, V. J. Polyak, J. B. T. Rasmussen, S. J. Burns, M. Lachniet, Multidecadal to multicentury scale collapses of Northern Hemisphere monsoons over the past millennium. *Proceedings of the National Academy of Sciences* **110**, 9651-9656 (2013).

Y. Asmerom, V. Polyak, S. Burns, J. Rassmussen, Solar forcing of Holocene climate: New insights from a speleothem record, southwestern United States. *Geology* **35**, 1-4 (2007).

W. E. N. Austin, F. D. Hibbert, Tracing time in the ocean: a brief review of chronological constraints (60–8 kyr) on North Atlantic marine event-based stratigraphies. *Quaternary Science Reviews* **36**, 28-37 (2012).

J. L. Banner, A. Guilfoyle, E. W. James, L. A. Stern, M. Musgrove, Seasonal variations in modern speleothem calcite growth in central Texas, USA. *Journal of Sedimentary Research* **77**, 615-622 (2007).

S. Barker *et al.*, Interhemispheric Atlantic seesaw response during the last deglaciation. *Nature* **457**, 1097-1102 (2009).

Barnett, Interdecadal interactions between the tropics and midlatitudes in the Pacific Basin - Barnett - 1999 - Geophysical Research Letters - Wiley Online Library.

J. L. Betancourt, T. R. V. Devender, P. S. Martin, *Packrat Middens: The Last 40,000 Years of Biotic Change*. (University of Arizona Press, 1990), pp. 482.

T. Blunier, Timing of Millennial-Scale Climate Change in Antarctica and Greenland During the Last Glacial Period. *Science***291**, 109-112 (2001).

E. Böhm *et al.*, Strong and deep Atlantic meridional overturning circulation during the last glacial cycle. *Nature* **517**, 73-76 (2015).

G. Bond *et al.*, Evidence for massive discharges of icebergs into the North Atlantic ocean during the last glacial period. *Nature* **360**, 245-249 (1992).

S. F. M. Breitenbach *et al.*, Constructing proxy records from age models (COPRA). *Climate of the Past* **8**, 1765-1779 (2012).

S. J. Burns, D. Fleitmann, A. Matter, J. Kramers, A. A. Al-Subbary, Indian Ocean climate and an absolute chronology over Dansgaard/Oeschger events 9 to 13. *Science* **301**, 1365-1367 (2003).

R. C. Casteel, J. L. Banner, Temperature-driven seasonal calcite growth and drip water trace element variations in a well-ventilated Texas cave: Implications for speleothem paleoclimate studies. *Chemical Geology* **392**, 43-58 (2015).

C. L. Castro, T. B. McKee, R. A. Pielke, The Relationship of the North American Monsoon to Tropical and North Pacific Sea Surface Temperatures as Revealed by Observational Analyses. *Journal of Climate* **14**, 4449-4473 (2001).

M. Center for History and New, Zotero Quick Start Guide.

J. B. Chapman, N. L. Ingraham, J. W. Hess, Isotopic investigation of infiltration and unsaturated zone flow processes at Carlsbad Cavern, New Mexico. *Journal of Hydrology* **133**, 343-363 (1992).

H. Cheng *et al.*, Improvements in 230 Th dating, 230 Th and 234 U half-life values, and U–Th isotopic measurements by multi-collector inductively coupled plasma mass spectrometry. *Earth and Planetary Science Letters* **371**, 82-91 (2013).

J. C. H. Chiang, C. M. Bitz, Influence of high latitude ice cover on the marine Intertropical Convergence Zone. *Climate Dynamics* **25**, 477-496 (2005).

S. L. Connin, J. Betancourt, J. Quade, Late Pleistocene C4Plant Dominance and Summer Rainfall in the Southwestern United States from Isotopic Study of Herbivore Teeth. *Quaternary Research* **50**, 179-193 (1998).

F. W. Cruz Jr *et al.*, Evidence of rainfall variations in Southern Brazil from trace element ratios (Mg/Ca and Sr/Ca) in a Late Pleistocene stalagmite. *Geochimica et Cosmochimica Acta* **71**, 2250-2263 (2007).

F. W. Cruz Jr *et al.*, A stalagmite record of changes in atmospheric circulation and soil processes in the Brazilian subtropics during the Late Pleistocene. *Quaternary Science Reviews* **25**, 2749-2761 (2006).

F. W. Cruz Jr *et al.*, Stable isotope study of cave percolation waters in subtropical Brazil: Implications for paleoclimate inferences from speleothems. *Chemical Geology* **220**, 245-262 (2005).

W. Dansgaard *et al.*, Evidence for general instability of past climate from a 250-kyr ice-core record. *Nature* **364**, 218-220 (1993).

P. Deines, D. Langmuir, R. S. Harmon, Stable carbon isotope ratios and the existence of a gas phase in the evolution of carbonate ground waters. *Geochimica et Cosmochimica Acta* **38**, 1147-1164 (1974).

J. A. Dorale, R. L. Edwards, E. Ito, L. A. Gonzalez, Climate and vegetation history of the midcontinent from 75 to 25 ka: a speleothem record from Crevice Cave, Missouri, USA. *Science* **282**, 1871-1874 (1998).

J. A. Dorale, Z. Liu, Limitations of Hendy test criteria in judging the paleoclimatic suitability of speleothems and the need for replication. *Journal of Cave and Karst Studies* **71**, 73-80 (2009).

R. L. Edwards, C. D. Gallup, H. Cheng, Uranium-series dating of marine and lacustrine carbonates. *Reviews in Mineralogy and Geochemistry* **52**, 363-405 (2003).

I. J. Fairchild *et al.*, Controls on trace element (Sr–Mg) compositions of carbonate cave waters: implications for speleothem climatic records. *Chemical Geology* **166**, 255-269 (2000).

I. J. Fairchild *et al.*, Modification and preservation of environmental signals in speleothems. *Earth-Science Reviews* **75**, 105-153 (2006).

I. J. Fairchild, P. C. Treble, Trace elements in speleothems as recorders of environmental change. *Quaternary Science Reviews* **28**, 449-468 (2009).

W. Feng, J. L. Banner, A. L. Guilfoyle, M. Musgrove, E. W. James, Oxygen isotopic fractionation between drip water and speleothem calcite: A 10-year monitoring study, central Texas, USA. *Chemical Geology* **304–305**, 53-67 (2012).

D. Gallego-Torres *et al.*, Rapid bottom-water circulation changes during the last glacial cycle in the coastal low-latitude NE Atlantic. *Quaternary Research* **81**, 330-338 (2014).

L. M. Gerhart, J. K. Ward, Plant responses to low [CO2] of the past. *New Phytologist* **188**, 674-695 (2010).

S. T. Gray, L. J. Graumlich, J. L. Betancourt, G. T. Pederson, A tree-ring based reconstruction of the Atlantic Multidecadal Oscillation since 1567 A.D. *Geophysical Research Letters* **31**, L12205 (2004).

M. L. Griffiths *et al.*, Evidence for Holocene changes in Australian–Indonesian monsoon rainfall from stalagmite trace element and stable isotope ratios. *Earth and Planetary Science Letters* **292**, 27-38 (2010).

E. C. Grimm, G. L. Jacobson, W. A. Watts, B. C. S. Hansen, K. A. Maasch, A 50000-Year record of climate oscillations from Florida and its temporal correlation. *Science* **261**, 198-200 (1993).

A. Guihou *et al.*, Late slowdown of the Atlantic Meridional Overturning Circulation during the Last Glacial Inception: New constraints from sedimentary (231Pa/230Th). *Earth and Planetary Science Letters* **289**, 520-529 (2010).

R. S. Harmon, H. P. Schwarcz, J. R. O'Neil, D/H ratios in speleothem fluid inclusions: a guide to variations in the isotopic composition of meteoric precipitation? *Earth and Planetary Science Letters* **42**, 254-266 (1979).

G. H. Haug, K. A. Hughen, D. M. Sigman, L. C. Peterson, U. Röhl, Southward Migration of the Intertropical Convergence Zone Through the Holocene. *Science* **293**, 1304-1308 (2001).

H. Heinrich, Origin and consequences of cyclic ice rafting in the northeast Atlantic Ocean during the past 130,000 years. *Quaternary research* **29**, 142-152 (1988).

S. R. Hemming, Heinrich events: Massive late Pleistocene detritus layers of the North Atlantic and their global climate imprint. *Reviews of Geophysics* **42**, RG1005 (2004).

S. R. Hemming, Heinrich events: Massive late Pleistocene detritus layers of the North Atlantic and their global climate imprint. *Reviews of Geophysics* **42**, (2004).

C. H. Hendy, The isotopic geochemistry of speleothems—I. The calculation of the effects of different modes of formation on the isotopic composition of speleothems and their applicability as palaeoclimatic indicators. *Geochimica et cosmochimica Acta* **35**, 801-824 (1971).

I. L. Hendy, The paleoclimatic response of the Southern Californian Margin to the rapid climate change of the last 60 ka: A regional overview. *Quaternary International* **215**, 62-73 (2010).

C. Hill, Overview of the geologic history of cave development in the Guadalupe Mountains, New Mexico. *Journal of Cave and Karst Studies* **62**, 60-71 (2000).

C. A. Hill, Sulfuric acid speleogenesis of Carlsbad cavern and its relationship to hydrocarbons, Delaware Basin, New Mexico and Texas (1). *AAPG bulletin* **74**, 1685-1694 (1990).

R. N. Hoy, G. W. Gross, "Baseline Study of Oxygen 18 and Deuterium in the Roswell, New Mexico, Groundwater Basin," (New Mexico State Univ., Las Cruces (USA). New Mexico Water Resources Research Inst., 1982).

E. W. James, J. L. Banner, B. Hardt, A global model for cave ventilation and seasonal bias in speleothem paleoclimate records. *Geochemistry, Geophysics, Geosystems* **16**, 1044-1051 (2015).

K. R. Johnson, C. Hu, N. S. Belshaw, G. M. Henderson, Seasonal trace-element and stable-isotope variations in a Chinese speleothem: The potential for high-resolution paleomonsoon reconstruction. *Earth and Planetary Science Letters* **244**, 394-407 (2006).

M. S. Lachniet, Climatic and environmental controls on speleothem oxygen-isotope values. *Quaternary Science Reviews* **28**, 412-432 (2009).

W. J. Lambert, P. Aharon, Controls on dissolved inorganic carbon and δ13C in cave waters from DeSoto Caverns: Implications for speleothem δ13C assessments. *Geochimica et Cosmochimica Acta* **75**, 753-768 (2011).

M. Latif, T. P. Barnett, Causes of decadal climate variability over the North Pacific and North America. *Science* **266**, 634-638 (1994).

Z.-H. Li, S. G. Driese, H. Cheng, A multiple cave deposit assessment of suitability of speleothem isotopes for reconstructing palaeo-vegetation and palaeo-temperature. *Sedimentology* **61**, 749-766 (2014).

M. Luetscher *et al.*, North Atlantic storm track changes during the Last Glacial Maximum recorded by Alpine speleothems. *Nature Communications* **6**, 6344 (2015).

M. Lyle *et al.*, Out of the tropics: the Pacific, Great Basin Lakes, and Late Pleistocene water cycle in the western United States. *Science* **337**, 1629-1633 (2012).

G. M. MacDonald, Water, climate change, and sustainability in the southwest. *Proceedings of the National Academy of Sciences* **107**, 21256-21262 (2010).

B. J. Macfadden, T. E. Cerling, J. M. Harris, J. Prado, Ancient latitudinal gradients of C3/C4 grasses interpreted from stable isotopes of New World Pleistocene horse (Equus) teeth. *Global Ecology and Biogeography* **8**, 137-149 (1999).

N. J. Mantua, S. R. Hare, Y. Zhang, J. M. Wallace, R. C. Francis, A Pacific interdecadal climate oscillation with impacts on salmon production. *Bulletin of the american Meteorological Society* **78**, 1069-1079 (1997).

F. McDermott, Palaeo-climate reconstruction from stable isotope variations in speleothems: a review. *Quaternary Science Reviews* **23**, 901-918 (2004).

J. S. McLean, "The Microclimate in Carlsbad Caverns, New Mexico," (1971).

S. Metcalfe, A. Say, S. Black, R. McCulloch, S. O'Hara, Wet Conditions during the Last Glaciation in the Chihuahuan Desert, Alta Babicora Basin, Mexico. *Quaternary Research* **57**, 91-101 (2002).

K. W. Meyer, W. Feng, D. O. Breecker, J. L. Banner, A. Guilfoyle, Interpretation of speleothem calcite δ13C variations: Evidence from monitoring soil CO2, drip water, and modern speleothem calcite in central Texas. *Geochimica et Cosmochimica Acta* **142**, 281-298 (2014).

P. J. Mickler *et al.*, Stable isotope variations in modern tropical speleothems: Evaluating equilibrium vs. kinetic isotope effects 1 1Associate editor: E. M. Ripley. *Geochimica et Cosmochimica Acta* **68**, 4381-4393 (2004).

G. E. Moseley *et al.*, Multi-speleothem record reveals tightly coupled climate between central Europe and Greenland during Marine Isotope Stage 3. *Geology* **42**, 1043-1046 (2014).

S. Nishizawa, D. R. Currey, A. Brunelle, D. Sack, Bonneville basin shoreline records of large lake intervals during Marine Isotope Stage 3 and the Last Glacial Maximum. *Palaeogeography, Palaeoclimatology, Palaeoecology* **386**, 374-391 (2013).

J. L. Oster, D. E. Ibarra, M. J. Winnick, K. Maher, Steering of westerly storms over western North America at the Last Glacial Maximum. *Nature Geoscience* **8**, 201-205 (2015).

J. L. Oster, I. P. Montañez, N. P. Kelley, Response of a modern cave system to large seasonal precipitation variability. *Geochimica et Cosmochimica Acta* **91**, 92-108 (2012).

L. C. Peterson, G. H. Haug, K. A. Hughen, U. Röhl, Rapid Changes in the Hydrologic Cycle of the Tropical Atlantic During the Last Glacial. *Science* **290**, 1947-1951 (2000).

J. S. Pigati, J. E. Bright, T. M. Shanahan, S. A. Mahan, Late Pleistocene paleohydrology near the boundary of the Sonoran and Chihuahuan Deserts, southeastern Arizona, USA. *Quaternary Science Reviews* **28**, 286-300 (2009).

V. J. Polyak, Y. Asmerom, Late Holocene climate and cultural changes in the southwestern United States. *Science* **294**, 148-151 (2001).

S. O. Rasmussen *et al.*, A stratigraphic framework for abrupt climatic changes during the Last Glacial period based on three synchronized Greenland ice-core records: refining and extending the INTIMATE event stratigraphy. *Quaternary Science Reviews* **106**, 14-28 (2014).

T. L. Rasmussen, E. Thomsen, M. Moros, North Atlantic warming during Dansgaard-Oeschger events synchronous with Antarctic warming and out-of-phase with Greenland climate. *Scientific Reports* **6**, 20535 (2016).

M. C. Reheis *et al.*, Directly dated MIS 3 lake-level record from Lake Manix, Mojave Desert, California, USA. *Quaternary Research* **83**, 187-203 (2015).

D. A. Richards, J. A. Dorale, Uranium-series Chronology and Environmental Applications of Speleothems. *Reviews in Mineralogy and Geochemistry* **52**, 407-460 (2003).

H. E. Ridley *et al.*, Aerosol forcing of the position of the intertropical convergence zone since ad 1550. *Nature Geoscience* **8**, 195-200 (2015).

B. A. Schubert, A. H. Jahren, The effect of atmospheric CO 2 concentration on carbon isotope fractionation in C 3 land plants. *Geochimica et Cosmochimica Acta* **96**, 29-43 (2012).

M. Schulz, M. Mudelsee, REDFIT: estimating red-noise spectra directly from unevenly spaced paleoclimatic time series. *Computers & Geosciences* **28**, 421-426 (2002).

R. Seager *et al.*, Model Projections of an Imminent Transition to a More Arid Climate in Southwestern North America. *Science* **316**, 1181-1184 (2007).

R. Seager, G. A. Vecchi, Greenhouse warming and the 21st century hydroclimate of southwestern North America. *Proceedings of the National Academy of Sciences of the United States of America* **107**, 21277-21282 (2010).

P. R. Sheppard, A. C. Comrie, G. D. Packin, K. Angersbach, M. K. Hughes, The climate of the US Southwest. *Climate Research* **21**, 219-238 (2002).

D. J. Sinclair *et al.*, Magnesium and strontium systematics in tropical speleothems from the Western Pacific. *Chemical Geology* **294**, 1-17 (2012).

J. D. Stanford *et al.*, A new concept for the paleoceanographic evolution of Heinrich event 1 in the North Atlantic. *Quaternary Science Reviews* **30**, 1047-1066 (2011).

I. T. Stewart, D. R. Cayan, M. D. Dettinger, Changes toward Earlier Streamflow Timing across Western North America. *Journal of Climate* **18**, 1136-1155 (2005).

D. M. Tremaine, P. N. Froelich, Speleothem trace element signatures: A hydrologic geochemical study of modern cave dripwaters and farmed calcite. *Geochimica et Cosmochimica Acta* **121**, 522-545 (2013).

D. M. Tremaine, P. N. Froelich, Y. Wang, Speleothem calcite farmed in situ: Modern calibration of δ18O and δ13C paleoclimate proxies in a continuously-monitored natural cave system. *Geochimica et Cosmochimica Acta* **75**, 4929-4950 (2011).

A. H. L. Voelker, Global distribution of centennial-scale records for Marine Isotope Stage (MIS) 3: a database. *Quaternary Science Reviews* **21**, 1185-1212 (2002).

C. Waelbroeck *et al.*, Sea-level and deep water temperature changes derived from benthic foraminifera isotopic records. *Quaternary Science Reviews* **21**, 295-305 (2002).

J. D. M. Wagner *et al.*, Moisture variability in the southwestern United States linked to abrupt glacial climate change. *Nature Geoscience* **3**, 110-113 (2010).

Y.-J. Wang *et al.*, A high-resolution absolute-dated late Pleistocene monsoon record from Hulu Cave, China. *Science* **294**, 2345-2348 (2001).

C. I. Wong, J. L. Banner, M. Musgrove, Holocene climate variability in Texas, USA: an integration of existing paleoclimate data and modeling with a new, high-resolution speleothem record. *Quaternary Science Reviews* **127**, 155-173 (2015).

C. I. Wong, D. O. Breecker, Advancements in the use of speleothems as climate archives. *Quaternary Science Reviews***127**, 1-18 (2015).

C. A. Woodhouse, D. M. Meko, G. M. MacDonald, D. W. Stahle, E. R. Cook, A 1,200-year perspective of 21st century drought in southwestern North America. *Proceedings of the National Academy of Sciences of the United States of America* **107**, 21283-21288 (2010).

C. J. Yapp, D/H variations of meteoric waters in Albuquerque, New Mexico, U.S.A. *Journal of Hydrology* **76**, 63-84 (1985).

H. Zhou *et al.*, Heinrich event 4 and Dansgaard/Oeschger events 5–10 recorded by high-resolution speleothem oxygen isotope data from central China. *Quaternary Research* **82**, 394-404 (2014).

APPENDIX SUPPLEMENTARY TABLES

Table S1: Stable Isotope time-series for BC-5

Age YBP	d13C	d18O	Age YBP	d13C	d18O	Age YBP	d13C	d18O
31005	0.02	-4.74	33182	-3.52	-5.07	35096	-4.32	-5.58
31048	-1.03	-5.73	33240	-3.60	-4.99	35194	-3.64	-5.50
31090	-1.09	-5.95	33298	-3.77	-5.13	35292	-3.29	-5.48
31133	-2.33	-6.05	33357	-3.26	-5.24	35390	-2.71	-6.05
31176	-3.46	-6.29	33396	-4.15	-5.69	35488	-3.71	-6.66
31218	-2.49	-5.78	33434	-3.84	-5.66	35586	-2.67	-6.30
31261	-1.93	-5.57	33473	-4.21	-5.83	35684	-1.65	-6.27
31303	-2.88	-5.97	33512	-3.97	-5.94	35782	-3.20	-6.93
31346	-3.12	-6.46	33551	-3.65	-5.83	35880	-2.88	-6.56
31389	-3.50	-6.09	33590	-3.64	-5.98	35978	-3.19	-6.89
31431	-2.58	-5.44	33628	-3.46	-5.92	36076	-2.78	-6.54
31474	-2.84	-5.26	33667	-3.19	-5.95	36174	-4.06	-6.81
31517	-1.91	-5.15	33706	-3.16	-5.88	36273	-3.38	-6.42
31559	-2.61	-4.97	33745	-3.50	-6.38	36373	-3.07	-5.79
31602	-3.65	-5.44	33784	-3.03	-6.03	36472	-3.74	-5.93
31644	-3.07	-5.13	33822	-2.68	-5.75	36572	-3.01	-5.62
31687	-4.05	-5.70	33861	-3.04	-5.93	36671	-3.21	-5.94
31730	-4.33	-5.69	33900	-3.39	-5.95	36770	-3.18	-5.84
31772	-3.88	-5.50	33939	-3.98	-6.42	36870	-3.34	-5.88
31815	-2.66	-5.05	33978	-3.49	-6.14	36969	-2.81	-5.64
31857	-1.71	-4.47	34016	-3.18	-6.20	37099	-3.50	-6.54
31900	-2.34	-4.71	34055	-2.28	-6.06	37228	-3.71	-5.45
31943	-2.09	-4.84	34094	-1.64	-5.85	37357	-2.18	-5.33
31985	-2.54	-4.66	34133	-2.60	-5.33	37487	-1.64	-5.12
32028	-2.55	-4.81	34172	-3.26	-5.40	37616	-1.52	-5.27
32070	-2.72	-4.83	34213	-3.04	-5.07	37746	-2.46	-5.48
32113	-2.92	-5.10	34254	-3.91	-5.33	37781	-2.71	-5.68
32156	-2.89	-5.12	34296	-4.16	-5.45	37817	-2.67	-5.61
32198	-1.51	-4.92	34337	-2.22	-4.84	37853	-2.70	-5.47
32249	-1.68	-5.06	34378	-2.53	-5.01	37889	-2.72	-5.50
32307	-2.06	-5.01	34420	-3.51	-5.53	37924	-2.54	-5.66
32365	-2.21	-5.08	34461	-3.02	-5.28	37960	-2.42	-5.75
32424	-1.84	-5.12	34502	-3.20	-5.33	37996	-2.90	-5.84
32482	-2.39	-5.40	34544	-3.15	-5.11	38032	-3.03	-5.83
32540	-2.31	-5.40	34585	-2.87	-5.19	38068	-3.21	-5.72
32599	-2.18	-5.10	34626	-3.08	-5.11	38103	-2.91	-5.56
32657	-1.52	-5.07	34668	-3.94	-5.40	38139	-2.80	-5.73
32715	-2.18	-5.13	34709	-3.93	-5.43	38175	-2.18	-5.23
32774	-1.99	-5.04	34750	-4.65	-5.90	38211	-2.15	-5.36
32832	-1.78	-5.09	34792	-5.03	-5.96	38246	-2.20	-5.58
32890	-1.82	-5.11	34833	-4.56	-5.51	38285	-2.59	-5.61
32949	-2.38	-5.29	34874	-4.20	-5.37	38323	-2.83	-5.80
33007	-3.45	-5.35	34916	-4.04	-5.31	38361	-2.82	-5.64
33065	-3.51	-5.29	34957	-4.25	-5.68	38399	-2.40	-5.84

Age YBP	d13C	d18O	Age YBP	d13C	d18O	Age YBP	d13C	d18O
38476	-3.20	-5.90	40687	-1.62	-5.86	43092	-4.00	-5.19
38514	-3.07	-6.23	40735	-1.66	-5.78	43109	-4.18	-5.45
38552	-3.83	-6.75	40783	-2.52	-6.15	43125	-4.12	-5.38
38590	-4.26	-7.25	40830	-2.15	-5.98	43141	-4.11	-3.65
38629	-4.16	-7.04	40878	-2.81	-6.35	43157	-4.34	-4.38
38667	-3.36	-6.60	40926	-1.97	-5.84	43173	-4.28	-4.34
38705	-3.83	-6.72	40974	-2.04	-5.88	43190	-4.23	-4.35
38743	-3.69	-7.05	41022	-2.60	-5.91	43206	-3.84	-4.07
38781	-3.31	-7.06	41070	-3.11	-6.16	43222	-4.15	-4.13
38820	-2.79	-7.12	41117	-3.12	-6.31	43238	-4.02	-4.34
38858	-1.53	-6.89	41183	-1.93	-5.59	43254	-3.54	-4.23
38896	-2.07	-6.80	41248	-3.21	-5.62	43271	-3.94	-4.43
38934	-3.45	-7.02	41313	-4.10	-6.26	43287	-3.69	-4.36
38973	-1.59	-5.98	41378	-3.60	-5.52	43303	-4.56	-4.72
39030	-3.24	-6.48	41444	-4.11	-6.31	43319	-4.68	-4.96
39088	-2.36	-6.42	41509	-3.79	-6.00	43335	-4.02	-4.85
39145	-3.52	-6.59	41574	-3.64	-5.87	43352	-3.90	-4.98
39203	-3.12	-6.35	41640	-3.45	-5.70	43368	-4.25	-5.30
39260	-3.27	-6.27	41705	-3.29	-5.53	43384	-4.79	-5.77
39318	-3.02	-5.90	41770	-3.15	-5.38	43400	-4.16	-5.36
39375	-2.99	-6.15	41835	-2.97	-5.36	43416	-3.89	-5.10
39433	-2.40	-6.44	41901	-4.17	-5.82	43432	-3.92	-5.27
39490	-2.33	-6.63	41966	-4.28	-6.06	43448	-3.87	-5.37
39548	-2.45	-6.53	42031	-3.55	-5.37	43464	-4.25	-5.67
39605	-4.05	-7.28	42097	-3.99	-5.51	43480	-3.88	-5.46
39663	-2.26	-6.46	42162	-3.85	-5.67	43496	-4.28	-5.65
39720	-2.33	-6.83	42227	-3.76	-5.32	43512	-5.10	-5.83
39778	-1.58	-6.83	42292	-3.58	-5.66	43528	-4.79	-5.46
39836	-1.77	-6.93	42358	-4.18	-5.01	43544	-4.76	-5.47
39893	-1.61	-6.26	42423	-4.59	-6.52	43560	-4.80	-5.40
39951	-1.93	-6.83	42488	-3.85	-5.97	43576	-4.64	-5.42
40008	-2.31	-7.09	42554	-3.50	-6.93	43592	-4.40	-5.45
40066	-1.59	-6.22	42619	-3.94	-6.98	43609	-3.92	-5.41
40113	-1.75	-6.13	42669	-3.97	-7.15	43625	-4.35	-5.69
40161	-2.51	-6.25	42704	-2.57	-6.15	43641	-4.62	-6.13
40209	-2.73	-6.26	42740	-2.57	-6.44	43675	-4.54	-6.45
40257	-3.26	-6.48	42775	-3.81	-6.28	43709	-4.95	-6.68
40305	-2.89	-6.60	42810	-4.25	-6.85	43744	-4.41	-6.55
40352	-3.95	-6.73	42845	-4.43	-6.56	43778	-4.43	-6.70
40400	-4.05	-6.86	42881	-3.68	-6.39	43813	-4.69	-6.82
40448	-3.35	-6.61	42916	-3.61	-5.85	43847	-4.79	-6.87
40496	-3.38	-6.65	42951	-3.48	-5.75	43881	-4.33	-6.63
40544	-2.06	-5.91	42987	-3.85	-5.63	43916	-4.18	-7.03
40591	-3.60	-6.30	43022	-4.09	-6.00	43950	-3.77	-6.55
40639	-3.18	-6.20	43057	-3.27	-5.23	43984	-4.15	-6.70

Age YBP	d13C	d18O	Age YBP	d13C	d18O	Age YBP	d13C	d18O
44019	-4.08	-6.76	52287	-1.48	-4.78	52951	-1.97	-4.44
44053	-4.19	-6.70	52304	-2.46	-4.58	52968	-2.15	-4.59
44088	-3.63	-6.30	52321	-3.96	-5.09	52985	-1.87	-4.53
44122	-3.12	-6.19	52338	-4.08	-5.23	53002	-1.89	-4.54
44156	-2.69	-5.98	52355	-3.76	-5.15	53019	-2.09	-4.52
44191	-3.08	-6.08	52372	-3.62	-5.19	53036	-1.84	-4.43
44225	-3.50	-6.17	52389	-3.31	-5.08	53053	-0.51	-4.07
44260	-3.58	-6.00	52406	-3.30	-5.17	53070	-1.62	-4.42
44294	-2.77	-5.58	52423	-3.07	-5.19	53087	-1.50	-4.38
44328	-3.79	-5.95	52440	-3.27	-5.18	53104	-1.71	-4.58
44363	-3.98	-5.93	52457	-3.61	-5.25	53121	-1.62	-4.36
44397	-3.98	-5.66	52474	-3.47	-5.14	53138	-0.56	-4.33
44431	-3.89	-5.52	52491	-3.60	-5.36	53155	-0.36	-4.49
44517	-3.76	-5.26	52508	-3.75	-5.29	53172	-0.25	-4.50
44603	-4.32	-5.52	52525	-4.19	-5.79			
44688	-4.30	-5.45	52542	-3.50	-5.49			
44774	-4.24	-5.20	52559	-2.89	-5.08			
44860	-4.28	-5.36	52576	-3.73	-5.19			
44946	-4.20	-5.14	52593	-2.69	-5.05			
45031	-4.29	-5.14	52610	-2.54	-4.92			
45117	-3.92	-5.29	52627	-2.97	-5.05			
45203	-3.80	-5.34	52644	-2.77	-4.96			
45288	-4.53	-5.36	52661	-3.02	-5.15			
45319	-4.09	-5.34	52678	-3.52	-5.05			
45350	-4.23	-4.97	52695	-3.73	-5.33			
45380	-4.67	-5.33	52712	-3.67	-5.12			
45411	-4.76	-5.40	52729	-4.04	-5.35			
45442	-5.04	-5.53	52746	-4.08	-5.44			
45473	-5.14	-5.76	52763	-3.21	-4.54			
45503	-5.11	-5.89	52780	-2.63	-4.80			
45534	-4.51	-5.65	52797	-1.39	-4.30			
45565	-4.65	-5.98	52814	-0.99	-4.49			
45595	-3.84	-5.61	52831	-1.26	-4.29			
45626	0.40	-4.86	52848	-0.45	-4.29			
45657	0.10	-4.68	52866	-0.91	-4.38			
Hiatus	**-**	**-**	52900	-1.75	-4.79			
52253	-1.11	-4.63	52917	-0.65	-4.52			
52270	-0.98	-4.45	52934	-0.16	-3.79			

Table S2: BC-5 trace element time-series reported in ppm

Age YBP	Mg	Ba	Sr	Age YBP	Mg	Ba	Sr
31005	6210	178.6	134.7	35096	6594	184.9	156.9
31090	5935	156.2	125.2	35292	6847	181.7	148.6
31176	5039	149.4	122	35488	7032	175.4	130.4
31261	5535	162.5	132.6	35684	6701	184.4	127.7
31346	6071	179.9	149.6	35880	7005	176	116.2
31431	5410	173.9	154.7	36076	5425	175.5	118.6
31517	5407	165.7	157	36273	6471	185.7	121.9
31602	5767	164.4	148.8	36472	7373	197.7	133.6
31687	5786	170.3	162.6	36671	7552	188.8	133.8
31772	5037	143.2	133.9	36870	7760	209.4	152.6
31857	6774	171.9	163	37099	8851	232	175.6
31943	6203	174.1	161.2	37357	7701	224.2	175.2
32028	6100	172.6	157.8	37616	7104	223.2	176.7
32113	7061	194.8	153.9	37781	7257	218.8	168.6
32198	6640	190.9	150.4	37853	6421	209.6	165.8
32307	6054	177.4	146.9	37924	7532	193.6	160
32424	6380	193.4	152.2	37996	7136	186	162
32540	6766	192.3	150.7	38068	6700	178.2	164.9
32657	6024	167.6	138.6	38139	7706	203.7	179.1
32774	6252	157.8	138.8	38211	7726	198	184
32890	5626	160.7	142.5	38285	7507	210.3	197.3
33007	5485	150.2	135.2	38361	8473	203.9	203.2
33123	5412	149.9	131.3	38438	5764	161	162
33240	6519	168.2	144.9	38514	5858	155	154.1
33357	5582	163.1	133.1	38590	6509	172.1	164.4
33434	4848	156.7	133.4	38667	6341	173.6	160.9
33512	5298	159.7	129.1	38743	6437	183.9	174.2
33590	5958	160.6	120.8	38820	6640	168.7	158.4
33667	5265	155.2	121.2	38896	5766	167.1	155.7
33745	5353	162.8	126.5	38973	5984	168.3	163.3
33822	6091	173.4	133	39088	6252	171.9	161.2
33900	5804	169.5	136.2	39203	5950	163.5	147.1
33978	6202	166	138.3	39318	6078	174.9	149.4
34055	5677	131.8	108.6	39433	5357	157.1	133.5
34133	5708	175.3	148.3	39548	5349	163	127.9
34213	5170	165	145.9	39663	5791	169.1	121.3
34296	5930	175.1	158.5	39778	5835	174.6	123.4
34378	5588	161.8	147.7	39893	5602	166.5	121
34461	6331	181.6	164.5	40008	5336	168.3	120.5
34544	5789	176.3	166.3	40113	6675	192	139.8
34626	6365	197.2	182.5	40209	6274	192.5	140.7
34709	4975	160.3	153.5	40305	5765	167.3	118.9
34792	4945	155.4	154.7	40400	7334	209	151.3
34874	5572	166.4	159.2	40496	5729	180.3	130.2
[illegible]	[illegible]	[illegible]	[illegible]	[illegible]	[illegible]	[illegible]	[illegible]

1166

Age YBP	Mg	Ba	Sr
40687	5177	173.2	134.5
40783	6609	194.3	142.8
40878	7451	216.2	154.6
40974	6492	214.6	147
41070	6866	221.4	158.5
41183	5866	184.1	134.9
41313	5390	168.2	133
41444	5386	171.7	131.4
41574	5105	167	134.3
41705	5238	160.5	130.8
41835	5403	171	137.2
41966	5293	171.8	131.4
42097	5908	177.6	144.9
42227	5704	178.4	134.4
42358	5607	172.8	137.5
42488	5886	186.7	137.1
42619	6449	193.5	132.2
42704	6612	187.1	131
42775	5344	173.4	124
42845	5506	178.1	129.8
42916	5612	191.1	133.9
42987	5963	209.1	147.3
43057	6777	214	164.6
43109	5537	171.7	141.4
43141	5516	176.9	143.7
43173	5764	191.9	158
43206	5089	181.3	155.6
43238	5433	182.6	156.5
43271	5632	172.1	139.7
43303	5518	187.3	152.3
43335	6038	202.6	181.9
43368	5154	181.4	154.7
43400	5418	189.8	166.7
43432	6692	213.7	182.1
43464	5475	198.8	171.4
43496	3756	133.6	113.5
43528	5235	176.9	153.3
43560	5278	181.7	154
43592	5995	190.4	163.7
43625	5161	169.3	142
43675	5443	169.4	138.6
43744	5281	168.1	127.2
43813	5307	168.6	131.6
43881	5830	184	131.2
43950	5633	181	134.5

Age YBP	Mg	Ba	Sr
44019	6645	209.7	148.6
44088	6196	196.5	135.2
44156	6364	221.5	147.6
44225	6010	192.1	140.7
44294	5758	188.7	147.4
44363	5963	203.7	153.2
44431	5869	197.6	146.7
44603	5787	184.9	145.5
44774	5479	177.3	143.9
44946	5934	190.6	145.5
45117	5437	176.6	140.9
45288	4861	174.4	135.5
45350	4741	173.2	133.7
45411	6567	214.1	170.1
45473	6479	195.3	154.2
45534	10730	250.2	185.8
45595	9964	273.3	218.1
45657	9203	259.9	214.5